POLITECNICO DI MILANO

School of Industrial and Information Engineering

Master of Science in Biomedical Engineering

Department of Electronics, Information and Bioengineering

POLITECNICO
MILANO 1863

DESIGN OF A URETEROSCOPE PROTOTYPE AND OF ITS PATH PLANNING STRATEGY

Supervisors: Prof. Elena De Momi
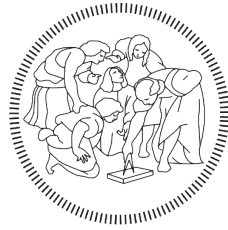   Prof. Dr. Jenny Dankelman
Assistant supervisor: Chun-Feng Lai, PhD candidate

<div align="right">

Master Thesis of:
Linda Scarzanella
student ID 916758

</div>

Academic Year 2019-2020

POLITECNICO DI MILANO

School of Industrial and Information Engineering

Master of Science in Biomedical Engineering

Department of Electronics, Information and Bioengineering

DESIGN OF A URETEROSCOPE PROTOTYPE AND OF ITS PATH PLANNING STRATEGY

Supervisors: Prof. Elena De Momi

Prof. Dr. Jenny Dankelman

Assistant supervisor: Chun-Feng Lai, PhD candidate

Master Thesis of:

Linda Scarzanella

student ID 916758

Academic Year 2019-2020

A Caterina

"To see the world,
things dangerous to come to,
to see behind walls, draw closer,
to find each other, and to feel.
That is the purpose of life."
The Secret Life of Walter Mitty

Ringraziamenti - Acknowledgment

The first big thank goes to Professors Elena De Momi and Jenny Dankelman, who made possible to work on my thesis project at TU Delft and always supported me. A special thanks goes then to Chun-Feng, who was my anchor during all those months, and to Pietro, whom I called seeking for help I don't even remember how many times when I felt more lost. He's a real genius but more, he become a friend (who makes incredible cakes).

Il mio più grande e sincero grazie, però, va sicuramente alla mia famiglia per tutto il supporto datomi in questi anni. Al mio papi, che ha sempre creduto nelle mie capacità, anche quando io ne dubitavo, che mi ha sempre spronato a non mollare mai, spinto a fare meglio ed ad andare oltre, anche quando questo significava lasciare il nido di casa. Alla mia mamma, una delle donne più cazzute che conosco – perdonami il francesismo - che mi ha insegnato, essendone lei esempio, che posso fare davvero tutto, anche da sola. Alla mia Cate: sei la mia pulcina, la mia sicurezza, la mia spalla e la mia giullare. Sei quella su cui poter sempre contare, in ogni occasione. Sei e sarai sempre la mia cucciola, anche se più di una volta sei stata tu quella forte e quella che mi dava la voglia e la forza di continuare. Non potrei descriverti che così: la metà esatta -identica e allo stesso tempo opposta- del mio cuore. E poi ai miei nonni, tutti e quattro, che mi hanno insegnato, dimostrandomelo, l'amore incondizionato (e anche quello per la buona cucina).

Un altro grazie va ai miei amici, con cui ho condiviso i più bei momenti di questi anni, e senza il cui perenne supporto avrei perso la sanità mentale. Ai Pijiati - Jessi, Aldino, Bomber, Pollo, Lanfra, Scara, Heinze, Baccio - con voi ho condiviso cene, vacanze ed eterne chiacchierate e discussioni ai Mercanti e al Baciccia, sempre comunque finite in risate con in mano una brioche di Bosoni. Alle tope - Anna, Clemi, Chiara, Marti, Marghe e Michi- che sono le amiche di una vita, da una vita. Con voi ho condiviso situazioni e luoghi (sotto un ombrellone di Riccione, in un Capodanno insieme a Parma, davanti a una birra ai Bikers in una sera qualunque) che hanno evocato confidenze che potevo fare solo con voi e che sono rimaste nostre, così come i momenti che abbiamo condiviso. Un grazie speciale lo devo alla mia persona, Anna, per esserci sempre: con un consiglio, un abbraccio, una risata, uno sguardo. A volte solo sapendo ascoltare e capire quello che vorrei dire senza riuscirci. Senza di te io non sarei io.

Grazie a tutti i compagni di università che ho incontrato in questi anni e con cui ho condiviso ansie, paure, giornate di stress, ma anche tante risate e qualche bevuta. In particolare, un enorme grazie a Fra, Rebe, Isa, Picci, Francesco e Dario. Un ulteriore grazie lo devo a tutti quelli de 'La Comune': Pietro, Paolo, Lore, Ami, Marghe, Livia, Fra, Ale, Andrea e Marco. Mi avete accolta nella vostra 'famiglia' e mi avete fatto sentire parte del gruppo pazzesco che avete creato. Tra grigliate, aperitivi, cene, spa, weekend in Belgio – e

mi fermo qui- avete fatto sì che questi mesi olandesi si siano trasformati in ricordi indelebili. Se la mia mancanza per l'Italia è stata minima è solo grazie a voi.

Un ultimo, immenso, grazie va alle due persone con cui ho convissuto durante i mesi della stesura della tesi, durante una pandemia globale: Eddi e Meme. Il vostro supporto – e la vostra sopportazione – sono stati immensi e ve ne sono infinitamente grata. Mi avete fatto sentire a casa, voi siete stati casa e per questo non potrò mai ringraziarvi abbastanza. Grazie Eddi, per i preziosi consigli, per le mille cene che mi hai cucinato, per gli insegnamenti sui cocktail e un po' anche per le battute non richieste. Sei fonte inesauribile di positività, grazie per averne sprizzata tanta intorno a me, soprattutto nei giorni e nei momenti in cui hai saputo capire che ne avevo più bisogno. E, *last but not least*, grazie Me, per tutte le chiacchierate, per quelle che hanno stimolato pensieri e per quelle che invece li hanno sbrogliati, per tutti gli abbracci, le canzoni che mi hai cantato, le bottiglie di Primitivo condivise. Tante volte mi hai capita anche quando io per prima non mi capivo. Sei la persona che in questo periodo della mia vita avevo bisogno di incontrare, perché grazie a te poi ho capito chi sono io.

Sommario

L'urolitiasi, ovvero la formazione di calcoli renali nel sistema urinario, è la terza patologia urologica più diffusa al mondo. Solamente in Italia, ad esempio, ogni anno vengono diagnosticati 100.000 nuovi pazienti. Quando i calcoli raggiungono una dimensione maggiore di 5 mm in diametro possono causare complicazioni, quali il blocco dell'uretere e dolore addominale, ed è pertanto necessario un intervento chirurgico per la loro rimozione. Attualmente, i calcoli vengono trattati con maggiore frequenza tramite le seguenti tecniche: litotrissia extracorporea a onde d'urto, nefrolitotomia e **ureteroscopia flessibile (detta anche fURS)**. La prima è una tecnica di chirurgia mininvasiva che sfrutta le onde d'urto per rompere i nefroliti in pezzi di dimensione minore, in modo tale che riescano poi ad essere espulsi tramite il tratto urinario. È una terapia efficace ma, talvolta, alcuni componenti chimici dei calcoli, come ad esempio monoidrato di calcio, brushite o cistina, sono resistenti alle onde, rendendo quindi inefficace il trattamento. La nefrolitotomia, invece, è una tecnica che prevede la rimozione dei calcoli tramite un endoscopio inserito in un'incisione che viene praticata nella schiena del paziente. Con questo intervento si riescono a rimuovere nefroliti anche di dimensioni maggiori; tuttavia, la tecnica risulta essere meno invasiva rispetto alle altre due. L'ureteroscopia flessibile, invece, consiste nel passaggio di un endoscopio flessibile che inserito nell'uretra del paziente e attraverso la vescica, raggiunge l'uretere, fino ad arrivare ai nefroliti.

Rispetto ai due precedenti trattamenti, la fURS ha il vantaggio di essere una tecnica mininvasiva, dato che sfrutta i lumi anatomici per il passaggio dell'endoscopio, riducendo quindi i rischi legati a possibili infezioni e i tempi di recupero del paziente. Questo metodo è inoltre sicuro e preferito per quelle categorie di pazienti considerati a rischio, quali donne in gravidanza, pazienti affetti da anomalie renali o in trattamento di anticoagulanti. Per queste ragioni, è la tecnica preferita in casi di calcoli di dimensioni intermedie.

La **difficoltà maggiore** durante l'intervento, riscontrata anche dai chirurghi più esperti, è la **localizzazione dell'orifizio ureterale (UO)**. Motivo per cui, prima della procedura, viene svolta una cistoscopia. Questo intervento viene svolto con un endoscopio inserito nella vescica del paziente, tramite l'uretra, per ispezionare la vescica con la camera dell'endoscopio, cercando di localizzare l'UO e incannularlo. Tuttavia, queste operazioni portare a due conseguenze. La prima è che, nonostante la cistoscopia, l'orifizio non venga localizzato, cosa che provoca il fallimento dell'intervento. La seconda è che, durante l'incannulamento, si danneggi l'orifizio o la mucosa intramurale, rendendo così ulteriormente difficile una successiva ureteroscopia.

Per cercare di superare i limiti dell'ureteroscopia, obiettivo di questa tesi è proporre un **prototipo di ureteroscopio** e creare una **strategia di *path-planning*** specifica. L'idea di fondo è quella di aiutare il chirurgo nel raggiungere l'orifizio, grazie alla proiezione di un percorso da seguire (creato *ad hoc* per il paziente) sullo schermo. In questo modo si tenta di ridurre il carico mentale del chirurgo ed evitarela cistoscopia.

Creare un robot flessibile pone delle richieste dipendenti dall'ambiente in cui andrà a muoversi e dal suo uso. In questo caso, il robot deve essere rigido assialmente in modo da avere un controllo affidabile ma allo stesso tempo deve essere flessibile e permettere curve in spazi tortuosi.

Deve inoltre essere manovrabile nelle due direzioni (destra/sinistra e alto/basso) e il suo controllo deve essere *user-friendly*.

Il prototipo è composto da due segmenti controllabili indipendentemente, ognuno dei quali possiede due gradi di libertà e da uno *shaft* rigido. È realizzato, in un solo step, tramite stampa 3D, ed è controllato tramite cavi. Questi sono collegati a motori stepper, comandati da joysticks. Poiché il progetto è ancora ad uno stadio iniziale, né fotocamere né altri sensori sono stati ancora integrati nel prototipo. Al momento, il prototipo viene direzionato manualmente. Suoi sviluppi futuri si focalizzeranno sul suo controllo automatico.

La strategia di *path-planning* ha l'obiettivo di guidare il chirurgo all'interno della vescica fino al raggiungimento dell'orifizio ureterale, passando per l'uretra. Nello stadio finale del suo sviluppo, infatti, il robot sarà in grado di muoversi autonomamente, seguendo il percorso sviluppato, per raggiungere l'orifizio. Attualmente, il prototipo viene mosso manualmente.

Poiché il *working space* è costituito da uretra e vescica, che sono tessuti molli e sono sottoposti a deformazione a causa della gravità e altri fattori, l'ambiente e possibili ostacoli non sono conoscibili a priori. Per sviluppare il *path*, per prima cosa è stato ricostruito un **modello virtuale di sistema urinario**, contenente vescica, ureteri e uretra maschili. I **parametri morfologici del modello**, come lunghezza e altezza della vescica, possono essere modificati e **customizzati per il singolo paziente**. Tali parametri, infatti, possono essere ricavati facilmente tramite l'analisi delle scansioni TAC del paziente. Tale esame diagnostico è infatti routine prima di un intervento di ureteroscopia. Il *path* viene creato poi basandosi su informazioni legate al modello. In particolare, l'algoritmo comprende due diverse fasi, una per ciascun organo che lo strumento deve attraversare (uretra e vescica). Durante

la permanenza nell'uretra, la strategia considerata ottimale è quella di mantenere il robot lungo l'asse centrale del lume, in modo tale da avere il minor contatto possibile con la delicata parete dell'uretra. Una volta entrato in vescica, il device segue un arco di circonferenza per raggiungere l'orifizio. Questa curva è stata scelta considerando l'alta flessibilità del prototipo e la sua facile capacità di seguire percorsi tortuosi. Il codice è stato scritto in Python.

Sono stati svolti alcuni esperimenti per testare se il controllo manuale potesse essere efficace nel muovere il prototipo, se questo potesse facilmente entrare nel modello di vescica in silicone, e se il *path* creato fosse in grado di far dirigere il prototipo verso l'orifizio.

La validazione della strategia e delle capacità del prototipo è stata fatta utilizzando dei fantocci di vescica creati col silicone, materiale che può riprodurre la deformabilità dei tessuti molli. Per validare il prototipo e il percorso creato con la strategia di *path-planning* sono state svolte due tipologie di prove. In entrambe la finalità dei partecipanti era quella di dirigere il prototipo verso l'orifizio ureterico del modello in silicone. Le prove sono state svolte da tre persone diverse, in modo tale da avere un *pool* di partecipanti maggiore. La prima tipologia consiste nel direzionare il prototipo verso l'orifizio del fantoccio seguendo le indicazioni di un utente (esterno) che ha la possibilità di visualizzare la scena. La seconda consiste nel muovere il prototipo seguendo il *path* sullo schermo, ove chi controlla i joysticks può vedere contemporaneamente sia la posizione attuale del sensore che il path creato automaticamente. Per ogni tipologia di prova, sia l'orifizio destro che il sinistro sono stati utilizzati come target. Ogni persona ha dovuto raggiungere ciascun orifizio 6 volte, 3 per ciascuna tipologia di prova.

Durante gli esperimenti, la posizione del primo segmento del prototipo è stata registrata tramite tracking elettromagnetico. Il percorso seguito

dal prototipo durante le due tipologie di prove è stato tracciato e comparato con il *path* creato. Inoltre, è stata calcolata la lunghezza di ogni *path* ed è stato svolto un test t di Student per valutare se la differenza in lunghezza nelle due tipologie fosse significativa. È stato inoltre registrato il tempo che ogni partecipante ha impiegato per lo svolgimento di ogni prova.

Dagli esperimenti fatti e dall'analisi dei dati acquisiti sono emersi sia aspetti positivi che possibili miglioramenti necessari. Il prototipo ha dimostrato essere facilmente controllabile, avere una corretta robustezza assiale e torsionale ma, allo stesso tempo, un'alta flessibilità. La strategia di *path planning* realizzata si è dimostrata essere un supporto visivo efficace per l'ingresso del prototipo nella vescica e per il raggiungimento della prossimità dell'orifizio ureterale. Nonostante sia emersa la necessità di alcuni possibili miglioramenti per il setup e la necessità dell'integrazione di alcuni sensori (es. sensori di forza per una possibile allerta quando superata la soglia oltre cui c'è un possibile rischio di danneggiamento alle pareti dell'uretra -necessari data la mancanza di un feedback tattile usando un controllo remoto-, una fotocamera endoscopica per l'aumento di visione), i risultati appaiono promettenti per proseguire la ricerca in questa direzione.

Abstract

The formation of kidney stones is the third most common urological disease worldwide. In Italy, every year 100.000 new patients are affected by kidney stones. The most common surgical procedures performed to remove the stones are Extracorporeal Shock Wave Lithotripsy (EWSL), Percutaneous Nephrolithotomy (PCNL), and **Flexible Ureteroscopy (fURS)**. EWSL is a minimally invasive surgery (MIS) technique that uses ultrasound waves to break up the stones into small pieces that can be then expelled in the urine. PCNL consists of the removal of stones using a scope inserted through a small incision performed in the back of the patient. It is efficient for large stones, but it is more invasive. fURS, differently, consist of the passage of a flexible endoscope, called ureteroscope, through the urethra and the bladder up to the ureter to collect and remove the stones. Compared to the first two interventions, fURS has some advantages. First, as it is minimally invasive, the risks of infection are minimized, and patient recovery is faster. Compared to EWSL, also a MIS, it has the advantage of being independent of the stone composition. In fact, some stone components (i.e. calcium oxalate monohydrate, brushite, or cystine) are not reactive to ultrasounds, thus leading to the failure of this technique. Moreover, fURS has been proven as the optimal choice for patients considered more fragile (i.e. pregnant women, patients affected by renal anomalies, and patients under anticoagulant treatment). For those reasons, fURS is the first choice

procedure in presence of intermediate size stones.

The main drawback of fURS is that **finding the ureter orifice (UO) is challenging** even for the most experienced surgeons. That is why they always perform a cystoscopy before fURS. A cystoscopy is an intervention where an endoscope is inserted in the bladder of the patient (passing through the urethra) to inspect the bladder. Surgeons, looking at the images reported by the endoscope camera, aim in trying to orient themselves in the bladder, to localize and cannulate the orifice. However, this can lead to two unfortunate consequences. The first is that, even with cystoscopy, sometimes the UO isn't found, and so the intervention fails. The second is that trying to enter and cannulate the UO can result in unwanted trauma to the orifice or intramural mucosa, making any subsequent ureteroscopy difficult. Moreover, many surgeons report orthopedic complaints, due to the suboptimal posture they're keeping while performing the interventions.

Trying to overcome the limits of fURS, this thesis proposes a design of a **ureteroscope prototype** and a **path planning strategy** specifically for it. The idea is to help the surgeon finding the orifice with the visual support of a pre-planned path, while he controls remotely the ureteroscope prototype. Having a pre-operative path, in fact, could reduce the surgeon's burden and cystoscopy could be avoided. Easing the task of finding the orifice, its cannulation wouldn't be necessary.

Designing a flexible robot comes with some challenges determined by its future environment and use. In this case, the prototype is required to have a small diameter, to have high axial stiffness to allow reliable control, and low bending stiffness to allow flexibility. It needs to have bidirectional maneuverability and its control needs to be user-friendly.

The prototype is composed of two independent steerable segments and

a rigid shaft. Each segment is steerable in two directions. The device is 3D printed in one step (no need of post-assembly) and is tendon-driven. Each segment is controlled by 4 tendons. Each tendon is controlled by a stepper motor. Motor control relies on joysticks. At this stage of research, the prototype is manually-driven. Next version of it will investigate automatic control.

The path planning strategy aims in helping the surgeon guide the ureteroscope in the urethra and the bladder of the patient, and in finding the UO. The working space of the robot is composed of the urethra and the bladder. Those organs are made of soft tissue, which easily undergoes deformation due to gravity and other factors. Therefore, an innovative path planning strategy was needed. The strategy is created by extracting information from a **rendered bladder model**, created using the average male urethra diameter and bladder height, length, and width. The **model** is **customizable**, in fact its morphological parameters can be adapted to each patient taking data from **CT scans**. CT scans are, in fact, commonly taken before such an intervention. The algorithm is made of two **different phases** that were adopted to adapt the algorithm to the **anatomic structure** involved in that part of the path. When the device is inserted in the urethra, being the diameter of the lumen small and the structure delicate, the path is created to make the device proceed along the axis of the lumen. This will prevent the device from hitting the walls of the urethra. When the device enters the bladder, the robot will proceed towards the UO. The orifice is located thanks to information extracted from the customized urinary system model. The code was written using **Python**.

Some validation experiments have been conducted. Three participants have been asked to perform the trials. Experiments were done to test if **human control could easily move the prototype**, if this one could

properly steer inside a phantom model and if the path designed could **guide participants in steering the prototype towards the orifice**.

Two different experiments were performed. The experiments consist of participants steering the prototype tip towards the orifice of a silicon bladder and urethra phantom model using two different strategies. During the first modality of the experiments, the participant is moving the prototype towards the target (= UO of a phantom bladder) while he/she is given directions from another user looking at the scene. During the second modality of the experiments, the participant has to reach the target (same as the one in the first modality) steering the prototype tip while looking at the computer screen. This displays the path designed and, superimposed to it, the real-time position of the tip. The segments of the prototype are controlled remotely by joysticks controlled by the participants. Both left and right orifices of the phantom model have been used as targets. For each orifice, three trials have been performed in each mode.

The tip position in space was recorded in all trials, exploiting electromagnetic tracking. The path made by the tip in each trial has been plotted, together with the path designed. The lengths of each path have been calculated, and a Student's T-Test has been performed to see if any statistically significant difference was present between the paths lengths of the two experiments. Moreover, the time needed in each trial to complete the task has been recorded.

The experiments and the analysis of the collected data enhance both promising and improvable aspects of this research. The prototype can steer easily in the phantom model and proves to be axially and torsionally stiff but flexible at the same time. The path designed guides the users correctly into the bladder and towards the proximity of the target. The

length of the paths recorded during the second experiment is lower, as the participants tend to be more focused and to not err when having to reach the target following the displayed path. However, the differences are not statistically significant.

The results not only appeared to be promising but they also threw light into future improvements and additions in the setup. For example, the integration of an endoscope camera and of a force sensor to alert risks of damage during the device insertion in the urethra could be of benefit and should be implemented in a future prototype.

Table of Contents

List of Figures

List of Tables

1

Introduction

1.1 Clinical background

Urolithiasis, also called nephrolithiasis, is the presence of stones formed in the kidneys and the urinary tract. It's the third most common urological disease worldwide affecting both women and men, with a prevalence of male patients. In the USA, people affected by urolithiasis are estimated to be 10% of the population [1]. In Italy, the percentage of the population affected by kidney stones is 6-9%, with 100.000 new cases every year, resulting in a total of 250.000 cases every year, comprehending relapsed patients [2]. From 2000 to 2010, in the UK, there has been an increase of 63% of people affected by upper urinary tract stones [3]. This increment, that affects all Western Countries, can be explained by the bad habits that have become more frequent in our lives: sedentarism, unhealthy diet, low intake of fluids. All those behaviors also brought to an increase in obesity, and obese patients have higher chances to be affected by kidney stones [4, 5]. Moreover, around 50% of the people

who had experienced the disease are going to be affected again during their lifetime, and so the recurrence risk is relatively high [6].

When the stones are smaller than 5 mm there is a 90% chance they will pass on their own. Differently, when they are bigger than 5 mm in diameter, they can cause complications (such as the block of the ureter), resulting in severe pain in the abdomen. When this occurs, surgical intervention is needed to remove the stones [7]. Before the '80s an open surgery was performed, but since the miniaturization of endoscopes - and in general of the medical instruments- using a minimally invasive approach became the gold standard. Minimally invasive surgeries (MIS) have lots of advantages compared to their open counterparts: lower risk of infection, lower recovery time, lower pain and discomfort, lower bleeding [8]. The preference of using a MIS can be seen in a study conducted in the UK: from 2000 to 2010 the number of ureteroscopies had an increase of 127%, while the number of open surgeries used for the same treatment decreased by 83% [3].

Nowadays, there are different techniques used to treat kidney stones, such as Extracorporeal Shock Wave Lithotripsy (ESWL), Percutaneous Nephrolithotomy (PCNL), and Flexible Ureteroscopy (fURS). EWSL is a minimally invasive surgical technique that uses ultrasound waves to break up the stones in small pieces that can be then expelled in the urine. This approach is usually preferred in case of small dimension stones. However, some stones composition (e.g. calcium oxalate monohydrate, brushite, or cystine) may limit the rate of success of the surgery. In fact, those types of stones tend to be less susceptible to EWSL, meaning they are more resistant and harder to break [9, 10]. PCNL consists of removal of the stones using a scope inserted through a small incision performed in the back of the patient [11]. This technique has a high success rate and it is used in case of large stones but is more invasive and for that avoided

when possible. Differently, fURS consists of the passage of a flexible endoscope through the urethra and the bladder up to the ureter to collect and remove the stones. It has minimal invasiveness and is the optimal choice in some cases where ESWL and PCNL would be less performant or even dangerous, such as in patients with bleeding diathesis, that takes anticoagulants, with renal anomalies, morbidly obese or pregnant. [1, 12, 13]

1.1.1 Ureteroscopy

Ureteroscopy is a procedure in which an endoscope, called ureteroscope is inserted through the patient urethra, bladder, up to the ureter, until the location of the stones. The patient is prepared in a dorsal lithotomy position and is under general or spinal anesthesia. Usually, ureteroscopy is a one-day routine surgery. [14]

The main medical device necessary to perform a ureteroscopy is an endoscope, called ureteroscope. In accordance with the specificity of the surgery, the instrument must fulfill specific requirements. The ureter has an average diameter of 1.8 mm (SD: 0.9, range 1-6 mm), usually being < 3 mm in asymptomatic people [15] . Therefore, the diameter of this endoscope must be small: it is usually asked to be smaller than 9 Fr (French gauge unit system, 1 mm = 3 Fr). Other requirements are optimal image quality of the image/video delivered, good irrigation, bidirectional maneuverability, minimal decrease of the urine flow rate with the administration of endoscopic tool, ergonomic and user-friendly handles to allow for torque and easily handling [4].

Moreover, other instrumentations are used when performing the surgery, such as a guidewire and a Ureteral Access Sheath (UAS). Guidewires help to have a safe introduction of the ureter catheter, and
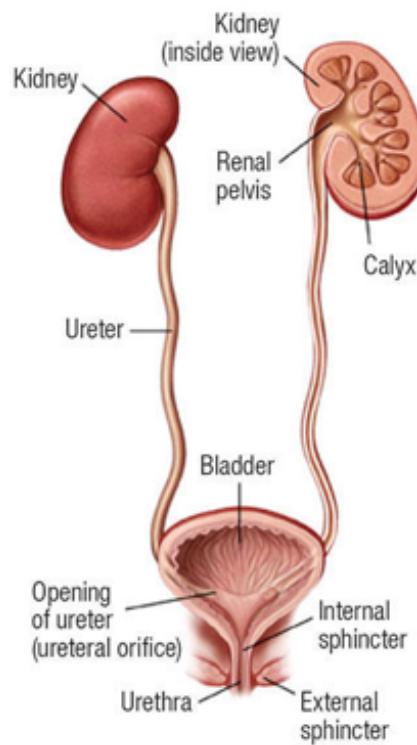
Figure 1.1: Urinary system.

so they must be a part of the medical devices used when performing this procedure [4]. While guidewires are well accepted, the usage of UAS is still a controversial point. Repeated entries and exit in the ureter cause lesioning, and therefore UAS is used to minimize this occurrence. On the other hand, UAS impacts the normal flow in the ureteral blood flow, leading to two major consequences: ischemia in the near future and damage via free radicals, which occurs after the reperfusion that follows the removal of the UAS [16, 17].

The first ureteroscopy was performed in 1912 by Hugh Hampton Young [18], who explored a dilated ureter. In 1964 Marshall was the first to use a flexible ureteroscope, created by Curtis and Hirshowitz [4]; it could only be passively deflected and didn't own a working channel. Another important step was taken in 1993 when Bangley performed the first ureteroscopy using a steerable-tip endoscope [19]. Back in those days, there were many limitations to the use of a flexible ureteroscope:

low angles of deflection, bad image resolution, difficult ureteral insertion [20]. Since then, with the miniaturization of medical instruments and the new studies about optical fibers, flexible ureteroscopes became popular.

1.2 Limits of ureteroscopy

One of the main causes of failure of ureteroscopy is not finding the Ureter Orifice (UO). Even experienced surgeons, in fact, have trouble in locating and visualizing it [21]. That is why, before ureteroscopy, a cystoscopy is performed. This intervention, performed with a scope inserted through the patient urethra and bladder, aims to explore the bladder thanks the help of an endoscopic camera positioned at the end of the scope used. This is done to localize the UO and cannulate it. However, this intervention can lead to two possible consequences. First, the orifice may not be found anyway. Secondly, repeated trials of entries of the orifice, while trying to cannulate it, can cause unwanted trauma to the orifice itself, or to the intramural mucosa [14], [22]. This would make difficult performing any subsequent ureteroscopy. Moreover, it is claimed that the standing ergonomic posture kept by the practitioner during ureteroscopy is a suboptimal one and may result in orthopedic complaints [23].

1.3 Goal of this thesis

Trying to overcome the current limits of ureteroscopy, the goal of this thesis is to design a **prototype of ureteroscope** and implement a **path planning strategy** specifically for it. The strategy designed in the thesis could help the medical practitioner guide the prototype to proceed towards the orifice. Moreover, having a pre-planned path

could reduce the burden of the surgeon. This way, the cystoscopy and the repeated trials of entrance of the UO, which can damage the orifice, can be avoided. In addition,the remote control of the ureteroscope could help surgeons improve the posture.

Therefore, this study include the development of a hardware part (the prototype) and a sofware one (the path planning algorithm).

Prototype. In accordance with the specificity of the surgery, this device, when enters in the bladder, is required to steer in a 3D environment without the support of the surrounding anatomy. At the same time, when it enters the ureter/urethra, the instrument must be adequately steerable not to damage the walls of the lumen but must be stiff to prevent unwanted buckling. The prototype should also be easy and intuitive to control by users. These examples make clear that there are many challenges involved in the development of this device. The prototype design will involve manual control, while further researches will investigate its automatic control.

Path planning algorithm. The path planning strategy designed aims to help the controller of the prototype guiding it towards the orifice. The visual support of the path should be enough to make the user guide the robot toward the orifice. The path is implemented using a rendered model of male urinary system, created using average data. This model can be adapted to each patient changing the bladder morphological parameters (i.e. frontal and lateral length, volume). This data can be extracted from Computer Tomography (CT) scans or ultrasounds of the patient anatomy, taken with routine exams performed before ureteroscopy. The starting point (in the urethra) and the target point (the ureter orifice - UO) will be located in the model. Thanks to a developed algorithm, a path between the start and the target points will be created. In designing the path, all the kinematics limitations of the instrument are considered.

2

State of the Art

2.1 History of ureteroscopes

In general, flexible endoscopes were developed as there was the need for an instrument for minimally invasive interventions that could proceed inside the tortuous lumen of the human body. The first attempts to develop steerable endoscopes appeared in the '50s, when Olympus Optical Company was asked for a camera to photograph and examine the inside of the human stomach [24]. After lots of research about the materials, the lens to use, and the mechanism, a prototype was developed. Unfortunately, the device wasn't suitable for practical clinical use. First reports of ureteroscopies appear in the '70s. Since then, many improvements and advancements in technologies have been made, leading to a complete change in the instrumentation and an increased rate of surgeries. From the '80s, flexible ureteroscopes started appearing more frequently in the OR. At the beginning, semi-rigid instruments were still preferred, due to the bad quality of the images and bad manoeuvrability of steerable instruments. With the miniaturization of the endoscopes and the development of fiber-optics technique, the flexible ones became the gold

standard instruments. Compared to the ureteroscopes available nowadays, those instruments were shorter (around 30 cm) and thicker. Even if they allowed a minimal invasive approach, their use was limited mainly to removal of proximal ureter kidney stones, as they were short and noted to damage the distal ureter. Over time they became longer (40+ cm) and thinner. The partial flexibility happened with the introduction of fibre-optics. The instrument is composed of fibre-optics bundles (fixed at both ends) and one or two working channels, all enclosed in a metallic shaft. Moreover, active deflection was introduced. Passive deflection consists in a non-rigid segment of the instrument that bends when in contact with the curves of the renal system. Differently, active deflection is present when the ureteroscope has a lever and cables mechanism that allows the surgeon to control the bending of the instrument. This kind of instruments are durable, and the main reasons of breakage is improper use or maintenance [19, 25–28].

2.2 Rigid, semi-rigid and flexible ureteroscopes

Rigid ureteroscopes were the first produced and used. Due to their rigidity, they couldn't reach the upper urinary tract and so, as soon as some technological improvement was achieved, they were substituted by semi-rigid ones.

semi-rigid ureteroscopes can have one or two working channels, which allow the simultaneous use of two instruments (i.e. one channel used for irrigation and one for a wire). When two working channels are present their diameters are usually 2.5 Fr and 3.4 (*Stryker* [29], [Figure 2.1]), or 3.6 Fr (*Dual Channel OES 4000, Olympus* [30]). When only one is present, its diameter is around 4 Fr. The working length of the shaft can vary; all of the companies analyzed in this research provide the same

instrument in a 33 cm and a 43 cm version. The diameter of the shaft is tapered in almost all the devices, except for the *Dual Channel OES 4000* by *Olympus*, which has a constant diameter of 7.5 Fr. The proximal diameter ranges from 7.5 (*Wolf, The Ultrathin* [31]) to 10.5 Fr (*Stryker*), while the distal one ranges from 6 to 6.9 Fr. [19]
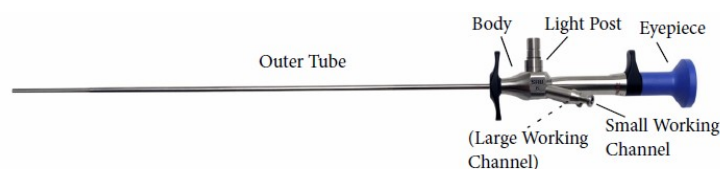

Figure 1: The Semi-Rigid Ureteroscope

Figure 2.1: Semi-rigid ureteroscope, Stryker Ⓡ.

Nowadays, flexible scopes are the most used when performing a ureteroscopy. Their high deflection makes possible to reach locations that couldn't be reached by rigid ones. Thanks to the research in the field of optic fibres, image quality improved tremendous. After 2000 the digital imaging system was introduced, bringing another great improvement in their image quality. In fact, in digital fURS the illumination can be made not only with fibreoptic bundles (such as in the fiber-optic fURS) but also by a diode. The image is then captured by a digital sensor located at the tip of the instrument [18–20].

Usually, flexible ureteroscopes have only one working channel, one or two fiber optic bundles incoherently arranged for light transmission, and one fiber optic bundle for image transmission. In the latests models the working channel is off-centered and its diameter is 3.6 Fr in most of the models. The length of the shaft can vary between 64, i.e. *ACMI DUR-8 Elite* [32], and 70 cm, i.e. *Olympus XURF-P5* [33], and the shaft is usually tapered. The size of the shaft at the proximal end varies between 8.4 and 10.1 Fr, while at the tip it varies between 6 and 7.5 Fr. The smallest diameter at the distal end is owned by the *Wolf 7325.076* [34]. The field of view in air varies between 80° and 90°. All recent models

possess an active deflection, which is reduced when a tool is inserted in the working channel. This doesn't limit their flexibility though, as evaluations report instruments are still able to deflect till 175°, which is the amount needed to reach lower-pole calices. The maximum active deflection is reported by the $Flex - X^2$, $Storz$ [35],[Figure 2.2], which can deflect ±270°. This is a great advantage and allowed the possibility to remove kidney stones even in the inferior calyx. One model, $ACMI$ DUR-8 $Elite$, has a double lever system, which allows secondary active deflection, reaching an S shape. The active bending mechanism consists of a pair of control cables running from the tip to a lever mechanism controlled by the surgeon and situated in the proximal end [19, 36, 37].

In the last few years, researchers started looking at the possibility of a robotic-assisted ureteroscopy. Saglam et. al. [23] designed the $Roboflex$ $Avicenna$, a prototype for fURS. The setup also included a surgeon's console and a manipulator for their innovative scope. They claimed that one of the problems encountered in this intervention is the suboptimal ergonomic posture of medical practitioners and tried to implement a solution for it. The evaluation of the prototype included seven experienced surgeons performing fURS on 81 patients. Despite some limitations encountered (i.e. lack of tactile feedback), promising results emerge from their research, which opens the door for robot-assisted fURS.

11278 A

Figure 2.2: Flexible ureteroscope, Storz ®.

2.3   Rigid VS flexible ureteroscopes

Many studies compared the procedure of ureteroscopy to remove
Proximal Ureteral Stones (PUS) with rigid and flexible instruments.
They all confirmed that fURS lead to a lower rate of complication than
RURS (Rigid Ureteroscopy). Here three examples:

- M. Ali Karadag et al. [38] comparing semirigid and flexible uretero-
  scopes stated that both the stone access rate and the reoperation
  rate with fURS was statistically better than with the semirigid in-
  strument (respectively 94% vs 76% and 6% vs 20.6%). The rates of
  complications were similar in both groups, but bleeding and ureteral
  internal injury were more common when the semirigid approach
  was used. Moreover, when the removal of kidney stones couldn't be
  possible during the semirigid intervention due to the tortuous path
  necessary to access it, fURS could be used to reach them.

- M. Galal et al. [39] compared rigid and flexible ureteroscopes. Their
  research results showed that even if the operation time was better
  in the study group in which a rigid ureteroscopy was performed, the
  success rate was better when a flexible endoscope was used (91% vs
  68%), along with the rate of intraoperative complication rate (9%
  vs 25%).

- E. Aklan et al. [40] also performed a case study comparing RURS
  and fURS. Their results stated that the worst handicap when us-
  ing rigid ureteroscopes was pushing a stone or its fragments back
  into the renal collecting system. Moreover, they noted that with
  fURS they could remove even coexisting renal stones. This can be
  one of the reasons for the higher average operation time of fURS
  respect to RURS. For what concerns the complications, even if
  statistically there were no difference in the complication rates of the

two groups, major complications (ureteral perforation and avulsion) occurred only when using a rigid instrument. They also stated that cost-effectiveness may be one of the reasons for the current use of rigid ureteroscope instead of flexible ones in many clinics. Most complications resulting from the usage of rigid ureteroscope derive from the impact of rigid instruments with the thin walls of the ureter, being it not straight but having curves both lateral to medial and posterior to anterior. Too much force given to the endoscope by the surgeon may result in damaging the instrument and in lesioning patients' anatomy (mucosal damage, perforation). The surgeon must be very careful not only during the insertion of the instrument but even during the removal of it from the patient. Therefore, even in the case of flexible instruments it can be seen the need for force sensors on the tip (and even -maybe- on the walls, to track and limit the shear forces) of the instrument, to limit the complications related to this surgery.

2.4   Control Mechanisms

Different control mechanisms have been studied to properly steer the endoscopes inside the tortuous path of the human body: magnetic, fluidic, cable-driven, telescopic, etc. The oldest actuation method is probably the one concerning fluidic actuation. The actuator is the compressor whose energy is transmitted by a fluid to articulations. K. Suzumori et al. [41], in 1991, created a robotic arm that included three internal chambers, and the internal pressure in each one could be controllable independently. This way, changing the pressure in the chambers, the robotic arm could be flexed in different directions. Another mechanism can consist of a shaft that can be telescopically extended. When the

parts that compose the shaft are pre-curved, this system can allow having curved paths. One example is the case of active cannulas [42]. One of the latest method used to control robots is exploiting the use of magnetic field to control a magnetically steerable catheter. The end-effector of those device houses a permanent magnet: this way using a magnetic field generator the robot can be moved and controlled. C. M. Heunis et al. [43] uses magnetic actuation to position an endovascular catheter: the dipole is attached to the catheter and it interacts with the magnetic field generated in a specific point in space. The current supplied by external coils allows the control of the actuation. S. Jeon et al. [44] developed a soft microrobot attached to the tip of a guidewire that is magnetically steered by changing the direction and the intensity of an external magnetic field.

However, the most commonly used technique of actuation makes use of cables [45]. Those are mechanisms with local actuation, where cables drive the different segments along the shaft of the endoscope. The cables respond to a handle-mechanism that the surgeon can control, a sort of a joystick that allows controlling the different DOFs of the instrument. For what concerns cable-driven endoscopes, another distinction can be made. Some articulations have compact joints, i.e. [46], while others are made of numerous joints, each with limited steering capacity. The latter are made to create longer and highly flexible instruments, such as in the endoscope developed by Gerboni et al. in [47]. There are even prototypes in which a set number of cables drive a specific segment, such as [48]. One of the main concerns about the latter type of mechanism is that cables controlling the most distal segments run along the whole shaft up to the handle. This results in the presence of a high number of segments in the proximal segments. Sometimes, this results in a conflict of movement and limits their ability to steer. One of the strategies to move those multiple segments endoscopes is the 'follow-the-leader' one

[Figure 2.3]. This strategy was originally developed by K. Asano et. al. [49] and allows having a snake-like motion. With this strategy, only the most distal segment of an instrument is actively controlled and directed, while the subsequent ones proceed on the path already traveled by the first segment. This mechanism can be thought of as a train with many wagons – each being a segment of the endoscope. The first wagon can put the rails ahead of itself, deciding the next move, while all the other wagons will follow the moves. Therefore, the first segment (= most distal) of the endoscope will move into a new position, while the second one will move towards the oldest location of the first one, and so on. This can be seen, for example, in the *Memoslide* [50]. It's a technique commonly used in endoscopic procedures. In fact, it can be used with a prior planned path as well as with manual exploration [51].
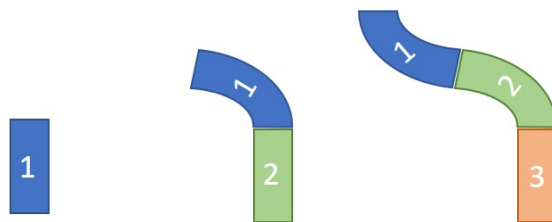

Figure 2.3: Example of follow-the-leader actuation. Control of the distal (1) segment of the endoscope sets the pathway for the subsequent segments (2 and 3) to follow.

2.5 Path planning strategies

Path planning is a crucial issue in the field of robotics, but the essence of this topic is 'just' a geometric problem: the need to find the optimal path between a starting and an ending point [52].

Nowadays, robots don't only have industrial use but are also appearing every day in our normal life. Therefore, since the problem of path-planning has become a very common matter lots of strategies were implemented. L. Yang et.al.[53] grouped and discussed the different 3D
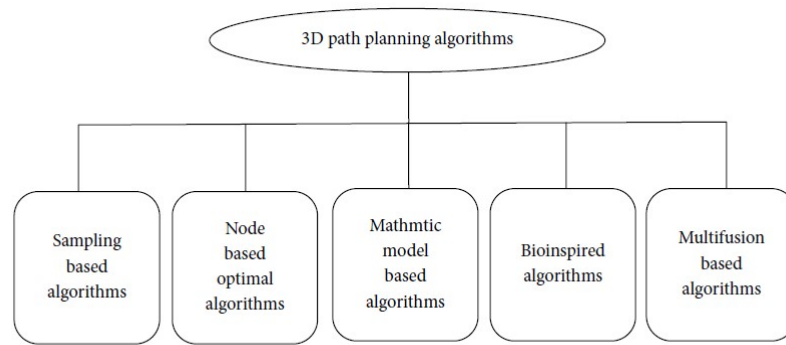
FIGURE 2: 3D path planning taxonomy.

Figure 2.4: Reprinted from "Survey of robot 3d path planning algorithm", by Yang, Qi, Song, Xiao, Han, Xia, 2016, Journal of Control Science and Engineering, Volume 2016, page 3.

path planning algorithms used in different fields of application. The most common algorithms are the *Node based optimal* and the *Sampling based* ones. A brief explanation of those two categories will be provided in the next two sections.

2.5.1 Node based optimal algorithms

The most used algorithms for surgery applications are the node-based ones. Different algorithms with different computational costs and efficiency belong to this group. The two most known are the Dijkstra and the A* algorithm.

The Dijkstra algorithm [54] starts with the assumption that all the points are infinitely distant from the start. Then, from the starting point, the algorithm checks all the neighbor points assigning to each a value. This value is the distance from that point to the start [See Figure 2.5]. It proceeds till it locates the target. Then, from the target, it starts scanning back all the points

Figure 2.5: Visualization of the Djkstra algorithm.

15

choosing at each iteration the one with the lowest value. The main disadvantage of Dijkstra is that it's not heuristic. It chooses only one of the possible paths available which may not be the most intuitive and preferable one.

An improvement was made with the creation of the A* algorithm [55]. It applies the same concept as the Dijkstra algorithm as it's also a cost-minimizing algorithm based on the same principle. However, at every step it uses a heuristic function: it calculates the distance (i.e. Manhattan or Euclidean distance) from the point where it is to the final point. This seems more a human way of thinking.

2.5.2   Sampling based algorithms

Sampling based algorithms are so-called as they sample the environment in which they are operating. The workspace has to be known a priori and needs to be described with mathematical equations. This allows to its sampling into cells or grids. The most common algorithms that fall into this category are the Rapidly-Exploring Random Tree (RRT) and the Artificial Potential Field.

RRT [56] is commonly used in 3D environments. It starts adding the starting node to a set that will contain all the nodes of the path. Then, it randomly chooses a node in the free space (q_{random}) and selects the closest node to it above the ones composing the path. This node will be called be q_{near}. Then, it tries to advance of a defined step in the direction q_{near}-q_{random}. If there are no obstacles in between, q_{random} will be added to the path. Otherwise, another q_{random} will be selected. This is done until reaching the target. This algorithm is called 'active' as it can decide on its own the best feasible path between the ones available.

16

The APF [57], differently, describes the workspace giving to cells a value corresponding to the potential energy of that region. Obstacles are surrounded by repulsive potential field while the target is surrounded by an attractive one [See Figure 2.6]. The algorithm, at every step, calculates the potential energy from there to the target and chooses the optimal path accordingly. The main problem of this algorithm is that the potential energy of the cells sums up during the calculation. This leads to an easily falling into local minimums.
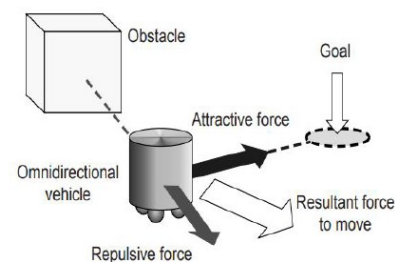
Figure 2.6: Reprinted from "Path Planning for Mobile Robots Using Potential Field Method", by D. Shah, 2018, Conference Paper.

2.5.3 Path planning strategies in medicine

In the last two decades, together with the miniaturization of devices and technologies developments, robot and computer-assisted surgeries have become more frequent. Those bring better results both to patients and surgeons. Patients experience less pain and have a faster recovery as the interventions are performed with small incisions instead of open surgeries. This already happened with laparoscopic surgeries [8]. Compared to them, though, having the support of a robot leads to a reduced mental burden for the surgeon [58], resulting in major results.

When the device is not driven manually, robots need paths to follow. Nowadays, several solutions can be found in the literature to solve the problem of path planning related to robotic medical instruments. The start and end points are usually set from CT scans, X rays, or assessed through fluoroscopy. To track the robot during his path different technologies and sensors are applied, such as magnetic ones. In this way,

with a closed-loop actuation, the path of the robot is checked against the planned one and corrected if necessary. In [59], Y. He et al. performed an endoscopic nasal surgery. First, they reconstructed a 3D model of the patient anatomy from CT scans and Magnetic Resonance Images (MRI). Then, again using the scans, they constructed a grid search map and applied the A* algorithm, estimating a specific cost function to minimize. In [60], F. Liu et al. elaborated a path planning strategy for prostate brachytherapy. They used MR images, segmented them, and reconstructed a 3D model of the anatomy of the patient. Then, trajectory planning was elaborated using an artificial potential field method. The basic idea is that the target point produces an attractive field, while the obstacles produce repulsive fields. In [61], Z. Zeng et al. used the A* algorithm to find the optimal path during a robot-assisted sinus surgery.
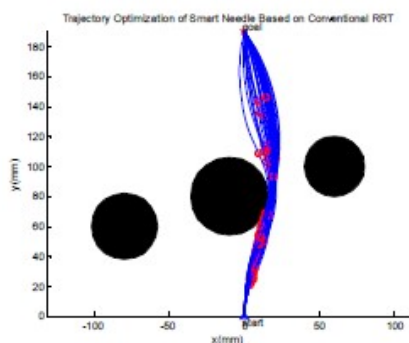

Figure 2.7: Path planning of a robot-assisted flexible needle. [1]

In this case, the model of the patient anatomy was reconstructed from CT scans, from which also the grid map was derived. The grid map was then manually modified to define some boundaries to lower the computational complexity. In another research, Y. Zhao et. al. [62] presented a method for designing the path for a steerable needle. The strategy used the RRT algorithm combined with the greedy heuristic strategy and the reachability guided strategy. Instead of searching for a generic node in between the start and the goal locations (as in the standard RRT) this solution tries first to connect the start and the end node with a straight line. If this is not possible because obstacles are present in between, the algorithm searches for the longest straight line possible which doesn't encounter obstacles. Then, it attaches it to a

---

[1]Reprinted from "path planning for robot-assisted active flexible needle using improved rapidly-exploring random trees", by zhao, joseph, yan et. al., 20142.7.

curved line which avoids the obstacles and reaches the target. Among the different paths available at the end of the search, an optimization function based on different parameters chooses the optimal one. [Figure 2.7] Moreover, other innovative strategies are present in literature when dealing with soft tissue and path planning. In [63], T. Bahwini et. al. defined a method to design a proper path when inserting a needle in presence of soft tissue. They modeled the tissue and its deformation in real-time using the finite element method. Then, a potential field of the environment was created using the modeling of temperature distribution. As the target was heated, it created an attractive spot. This way the optimal path could be implemented. A different solution for the same problem was thought by Y. Zhao et. al. [64]. Once calculated the kinematics of the needle, they first applied an RRT algorithm combined with the greedy heuristic method and the reachable guided strategies to define the optimal path. This first step was done using medical images (CT and MRI) of the patient. Then, they did a re-planning intraoperatively to perform a sort of closed-loop control: online medical images were used to systematically correct the path at every loop till reaching of the target region.

3

Materials and Methods

Flexible ureteroscopy, being a minimally invasive surgery and safer in different categories of patients, is usually the optimal choice for the treatment of intermediate size nephrolithiasis. One of the problems faced even by the most experienced surgeons during this intervention consists in finding the UO. For this reason, the surgery is usually preceded by a cystoscopy which aims at exploring the bladder and cannulate the orifice. Surgeons 'just' look at images of the endoscopic camera and try to find the orifice. Even with this previous intervention, sometimes surgeons can't find the orifice. If they find it, when they're trying to cannulate it, they may damage the orifice or the intramural mucosa, making any subsequent ureteroscopy very difficult.

For this reason, this thesis proposes a **ureteroscope prototype** that can be remotely controlled, and a **path planning strategy** designed specifically for it, to **help surgeons in finding the orifice** avoiding the cystoscopy. Let's see more in details both the hardware and the software developed.

<u>**Hardware**</u>. The flexible robot must be reliably controllable, but also be flexible enough to steer in a tortuous path. It's composed of two

steerable segments and a rigid shaft. The segment's body structure is the same as the one of the *HelicoFlex* [65] robot, but its dimensions have been adapted to cope with the requirements needed for a ureteroscope. The prototype is tendon-driven and is controlled remotely thanks to joysticks. The remote control allows the surgeon to sit in a better ergonomic position respect to the suboptimal posture which is usually assumed during the standard ureteroscopy.

Software. A path planning strategy was made by this researcher to help the surgeon from the urethra to the orifice, in order to enter the correct side of the bladder and find the UO. Having a pre-planned strategy could also reduce the mental burden.

A male urinary system has been modeled for the path planning. It's customizable; in fact, its morphological parameters can be changed extracting data from CT scans relative to the patient bladder (height, width, and length). CT scans are, in fact, always taken before ureteroscopy. The path planning strategy designed for the instrument prototype is different depending on which part of the urinary system it is currently passing through. In the urethra, the path is developed to make the device avoid as much as possible contacts with the lumen walls. When the instrument enters the bladder, an arc of circumference is used to reach the orifice.

In this section, the prototype design, the bladder model design, and the path planning development and its results are explained.

3.1   Ureteroscope prototype

The need for steerable devices that can better adapt to the tortuous lumen present in our body is nowadays a known problem. Therefore, more advanced instrumentation presents different flexible parts. This

characteristic is also present in the design of the prototype presented in this thesis. It can be thought of as an invertebrate animal, as it can form continuous curves [66].

3.1.1 Requirements

The prototype must fulfill the requirements needed for this specific scope, which are [4]:

- Diameter $\varnothing < $ **3 mm**, to cope with ureter diameter ($\approx$3 mm for patients affected by nephrolithiasis);

- Radius of curvature $\rho \leq $ **20 mm**;

- **Bidirectional** manoeuvrability;

- **Ergonomic** and **user-friendly** (to allow for torque and easy handling);

3.1.2 Design

A prototype of endoscope, called in *HelicoFlex* robot [65] [Figure 3.1], developed by the BITE group [66] at TU Delft [67] presented high torsional and axial stiffness and low bending stiffness. As the characteristics seemed promising, it was chosen to use the same segment body structure present in it, changing its dimensions to cope with our goal. The prototype segments body is then composed of a continuous central backbone around which a helicoid runs [Figure 3.2]. The central element provides high axial stiffness, while the compliant helicoid element provides high torsion stiffness and low bending stiffness due to its intrinsic structure. As the pitch of the helicoid element is the same as the length

---

[1]Reprinted from "Exploring non-assembly 3D printing for novel compliant surgical devices", by Culmone et.al., PLoS One, 2020.

Figure 3.1: Helicoflex robot.
[1]

of each segment, four helicoids were placed around the backbone to have a more homogeneous stiffness compared to only one [Figure 3.2c].

The prototype is composed of two steerable segments and a rigid shaft [Figure 3.4]. Each segment is bendable, independently controllable in 2 DOFs and has a length of 2 cm. The shaft is rigid, not controllable, and it is 6 cm long. The shaft length was chosen by this author, according to the necessity to insert the instrument in the urethra and the bladder till the UO. The **backbone** has a diameter of **0.8 mm** [Figure 3.2c.1], while the **total diameter** of the prototype is **5 mm**. With only two steerable segments present in this design, the maximum **angle** achieved is **120°**. The radius of curvature (ρ) resulted to be **19 mm**. It has
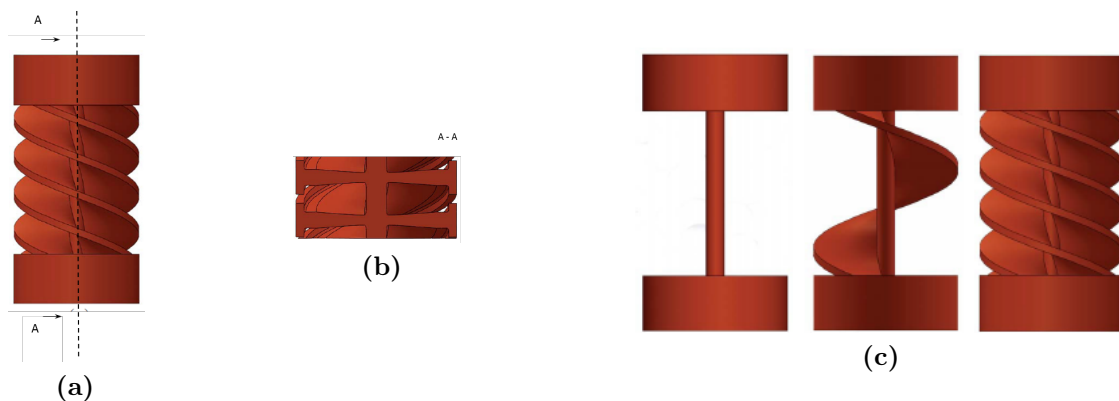
Figure 3.2: Drawing of the prototype structure (a) and its section A-A (b) to enhance the backbone and the helicoid structure. The structure presents a backbone (c.1) around which are placed four helicoid elements (c.3). In c.2 one pitch element is enhanced. [2]

been then calculated with the following equation, with A = 4 cm and *theta*= 120°.

$$\rho = \frac{180 \cdot A}{\pi \cdot \vartheta} \tag{3.1}$$
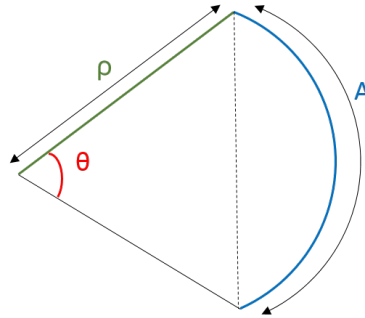
Figure 3.3: Measure of curvature. A:arc of circumference, ρ: radius, ϑ: angle.
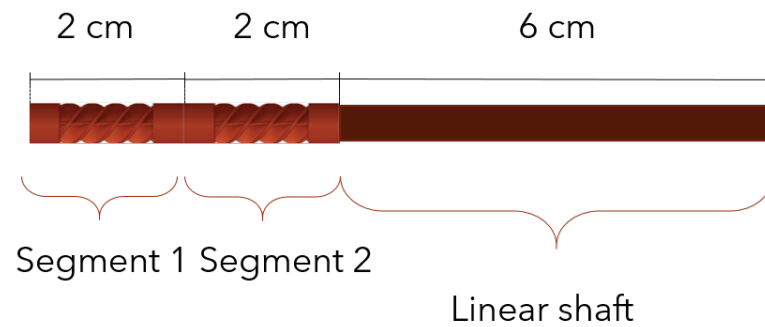

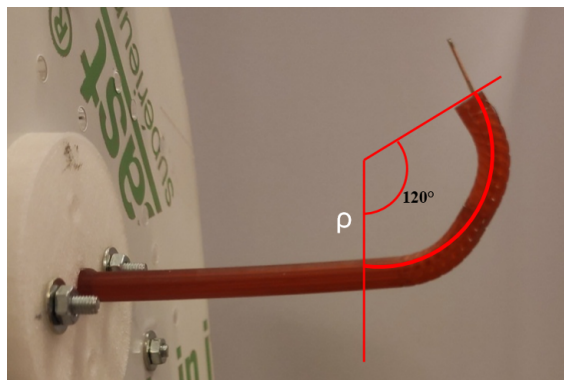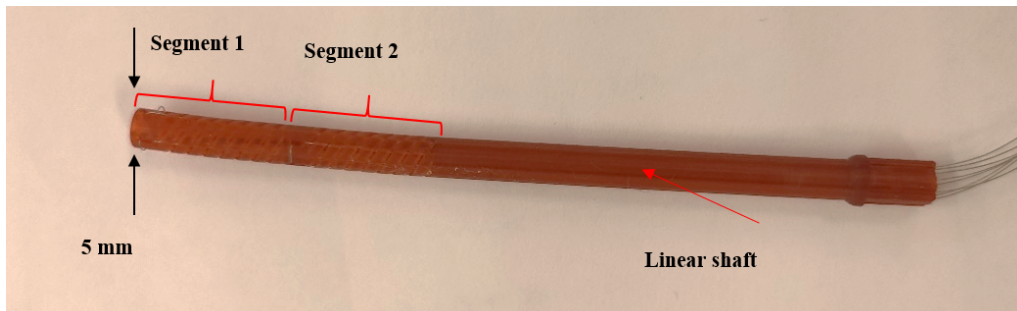**Figure 3.4:** Schematic drawing of the prototype design.

Figure 3.5: Visualization of max deflection angle of the prototype.

---

[2]Reprinted from "Exploring non-assembly 3D printing for novel compliant surgical devices", by Culmone et.al., PLoS One, 2020.

Figure 3.6: Prototype image.

3.1.3 Control

There are many different methods of control of steerable instruments, such as hydraulic, pneumatic actuation, shape memory alloys etc. Tendon-driven actuation remains the most used one.

Therefore, this method was used even in this application as it allows the control of multiple DOFs while keeping the size of the tip small. Each steerable segment is controlled by 2 cables (four tendons), as can be seen in Figure 3.8. The choice was to use a cable fixation method that could avoid soldering or gluing in the shaft. Two cables per segment were used. The cables

(a) Top view

(b) Frontal view

Figure 3.7: Schematic drawing of 3D printed shaft and assembling cables in yellow. [3]

used have a diameter of 0.15 mm and a tensile strength of 1770 MPa. Each cable run in the grooves along the segments and the shaft. In the top of each segment it loops inside a cross-shaped groove in the transverse plane of the segment and bends its ends 90° in the pulling [Figure 3.7 and 3.8]. At the end of the shaft, each tendon is fixed to the pulley of stepper motor [Fig. 3.8]. The specifications of the motors can be found in their datasheet [68]. The stepper motors are arrayed with
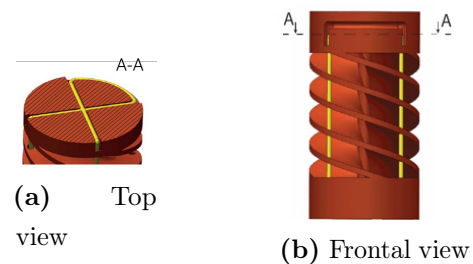
---

offset angles to minimize the space required for each motor [Fig. 3.9]. Mechanical supports and actuators are identical for each segment. The choice was to use modular actuation. In fact, modular actuators allow to easily control more DOFs while being flexible for different designs. Using a high number of motors is usually not advisable as they require sterilization and unsustainability for disposable devices. However, as it's
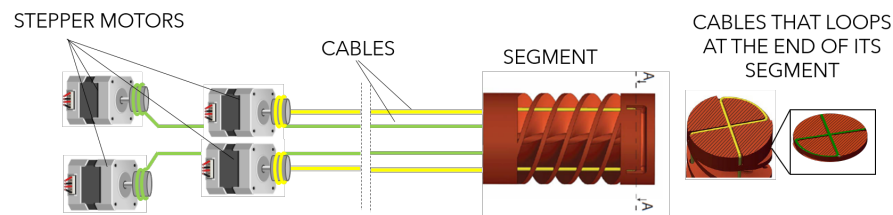

Figure 3.8: Schematic of the cable-driven system that controls each segment motion. Each cable is inserted in the transverse plane of the segment, where it loops inside a cross-shaped groove. Both its endings run in the dedicated grooves along the segment and the shaft and end on the pulley of a stepper motor.

still at an early stage of research, this prototype now is not ready for clinical environments, and its setup was created to test the prototype motion. At this stage of research, the DOFs are controlled by joysticks [Figure 3.11]. Each joystick controls the 2 DOFs of one segment [Fig. 3.10a]. As the prototype is composed by two segments, 2 joysticks are necessary. To move the tip in one of the four possible direction (up, down, left or right as can be seen in Figure 3.10b), two tendons are pulled, and so two motors are actuated at the same time. As are the joysticks that steer the prototype, this remote control could allow the surgeon to sit in an ergonomic position, solving the orthopedic complaints due to a suboptimal posture pointed-out in some studies [23].

The prototype is mounted on acrylic-panel support that enables it to be standing and having enough space for steering in three dimensions [Figure 3.11]. The button of each joystick exploits then the control of the slide, allowing the prototype to move in the third direction (so it can move back and forth). The panel replicates the two panels that hold
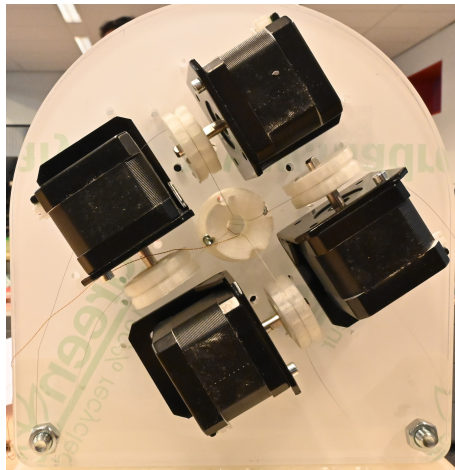
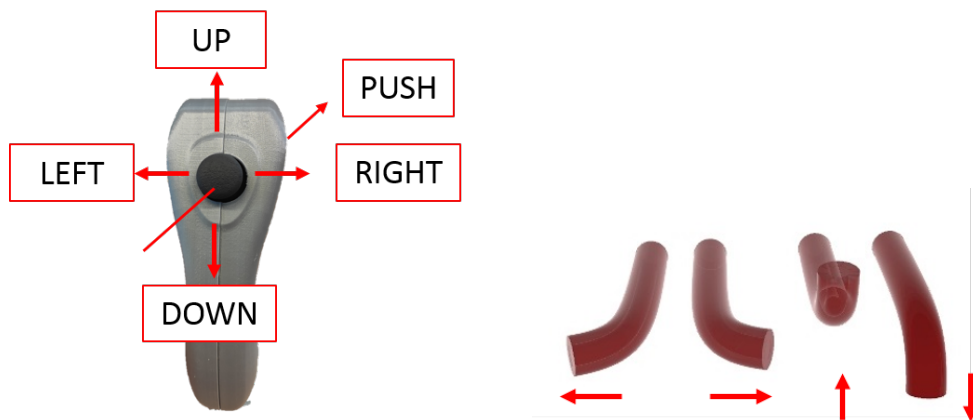**Figure 3.9:** Motors controlling segment.

Figure 3.10: (a) Possible movement of the joystick controller. Right, Left, Up and Down control the same movement on the tip. The button, when pushed, controls the motion of the panel on the linear slide. (b) Rendered prototype to show the four directions of movement.

the motors. All panels are then screw-fixed to a platform mounted on a slide. As the segments have only 2 DOFs, the slide is necessary to achieve movements in the third dimension.
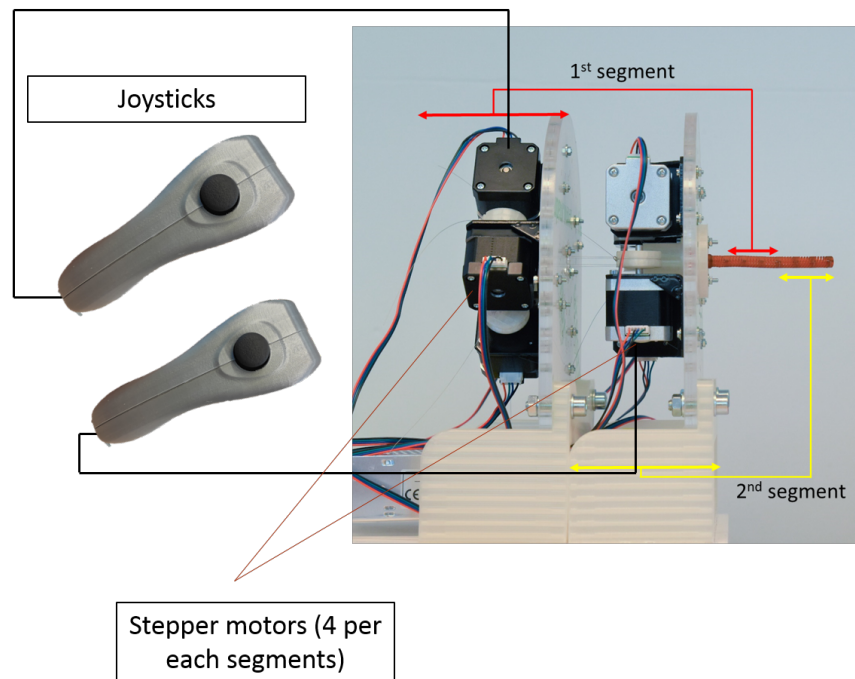
Figure 3.11: Prototype setup schematic.

3.1.4 Performance indicators

The prototype has a **external diameter of 5 mm**. This value can be compared to those of cystoscopy instruments, whose diameter is approximately 5 mm. Future development will inquire further miniaturization to compete with nowadays ureteroscopes. The maximum angle of deflection (ϑ) is **120°**, which is more than the maximum value found in the path planning strategy designed. Additional deflection could be achieved implementing a high number of segments in the design. The radius of curvature ρ resulted to be ~ 19 mm, consistent with the requirements. Each segment can steer in 2 DOFs, therefore allowing **bidirectional maneuverability**. Joysticks are exploited for its control, as they appear being **ergonomic and user-friendly**. This aspect will be evaluated in the experiments.

3.1.5 Fabrication

The prototype was 3D printed in one step. The choice to use Additive Manufacturing (AM), also called 3D printing, was made as it has some great advantages. AM directly prints CADs, allows the production of complex geometry, is faster and less expensive than other techniques [69]. Moreover, the prototype is non-assembly, meaning that is all printed in one step with no necessity of subsequent steps for its assembly. This conveniently reduces the post-processing time. As the dimensions of the prototype are considerably small, a high-resolution printer was needed. Perfactory®4 Mini XL (EnvisionTec GmbH, Gladbeck, Germany), with a layer height in the vertical z-axis of 25 μm, was used. The used printer is based on photopolymerization technology and uses the so-called Digital Light Processing (DLP) in which the combined work of a light source and a projector hardens the liquid resin layer by layer [70]. The prototype was printed using the R5 epoxy photopolymer resin. All the properties of this material can be found in [71]. This resin is not biocompatible. Some bio-compatible resins are available at Envision-Tec. However, as reported by Culmone et al. in [65], a trial of printing the *HelicoFlex* robot with some biocompatible resins was made but resulted in a non-decent result due to the high viscosity of the resin, which made cable grooves more difficult to be printed. Other types of bio-compatible resins will be investigated in the future.

3.2 Urinary system model

The urinary system model created for the path planning strategy was designed with the software Rhinoceros 3D (Rhino ®) [72]. Rhino is a 3D computer graphics and computer-assisted-design (CAD) application

software. It has many different applications such as modeling, rendering, and animation. It has plug-ins that facilitate 3D printing and it allows to save models in 3D-printer compatible file formats.

The model is designed assuming the bladder as an ellipsoid, and considering the average volume and length of an adult male bladder, which is ∼350 ml, while the average length is 10 - 12 cm [73]. The bladder can be modeled as an ellipsoid, for which:

$$Volume = Length \ \times \ Width \ \times \ Height \ \times \ 0.52$$

The morphological parameter such as the average lengths (frontal and lateral) and height can be changed to adapt the model to a specific patient. Those values can be obtained through CT or ultrasound scans of the
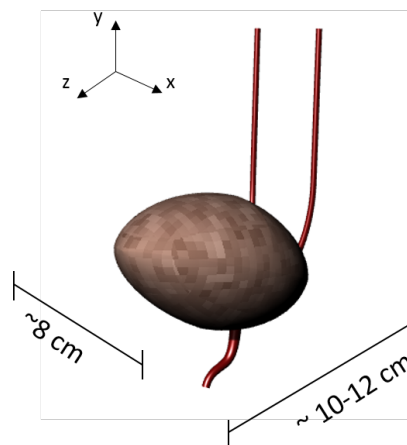

Figure 3.12: Rendering of a urinary system model using average male urethra, bladder, and ureters dimensions. Its parameter are customizable using information that can be extracted from patients CT scans.

patients. Those are routine exams when investigating for kidney stones. CT scans are contained in DICOM format images. Using dedicated programs (i.e. Slicer [74]), the scans can be uploaded and the ones containing the bladder can be seen and used to construct customizable bladder models.

The ureters are designed as 4 mm tubes inserted in the posterior

bladder, idealistically in the trigone [Figure 3.13]. The insertion of the urethra was reconstructed taking into accounts the male anatomical model of bladder and urethra. When entering the bladder model, the latter has a diameter of 6 mm. The generic reconstructed model can be seen in Figure 3.12
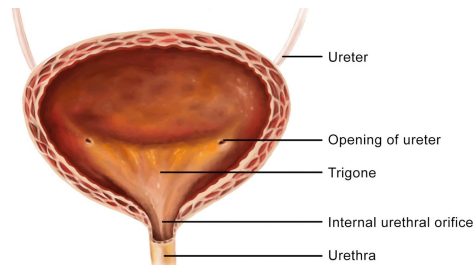

Figure 3.13: Bladder anatomy.

The model has been saved as an OBJ file. OBJ is a file format for 3D objects which contains information about the vertex position, faces of the model, and vertex normals. To reconstruct the model with the code, a triangled-meshed model was performed. Therefore,

Figure 3.14: Example of a sphere in OBJ file with triangular meshes.

a triangularization of the meshes composing the file was necessary. This way, the OBJ file contained the set of coordinates relative to the vertexes of triangles forming the model. [see Figure 3.14].
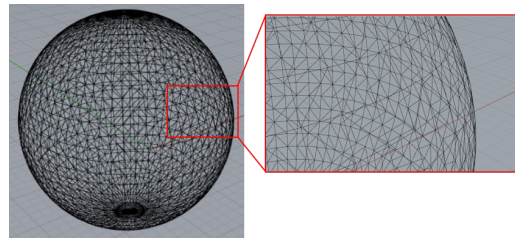
3.3 Path Planning

The path planning strategy is designed for the prototype described in the previous section. Therefore, it needed to consider its specifics. In particular, its radius of curvature ($\sim$ 20 mm) the maximum angle of deflection (120°) and the length of each segment (2 cm).

The code is written in Python. In Figure 3.15 a flow chart of the code is represented. As can be seen from the flow chart, before starting with the path planning strategy, few steps were performed to reconstruct the bladder model from the OBJ file.
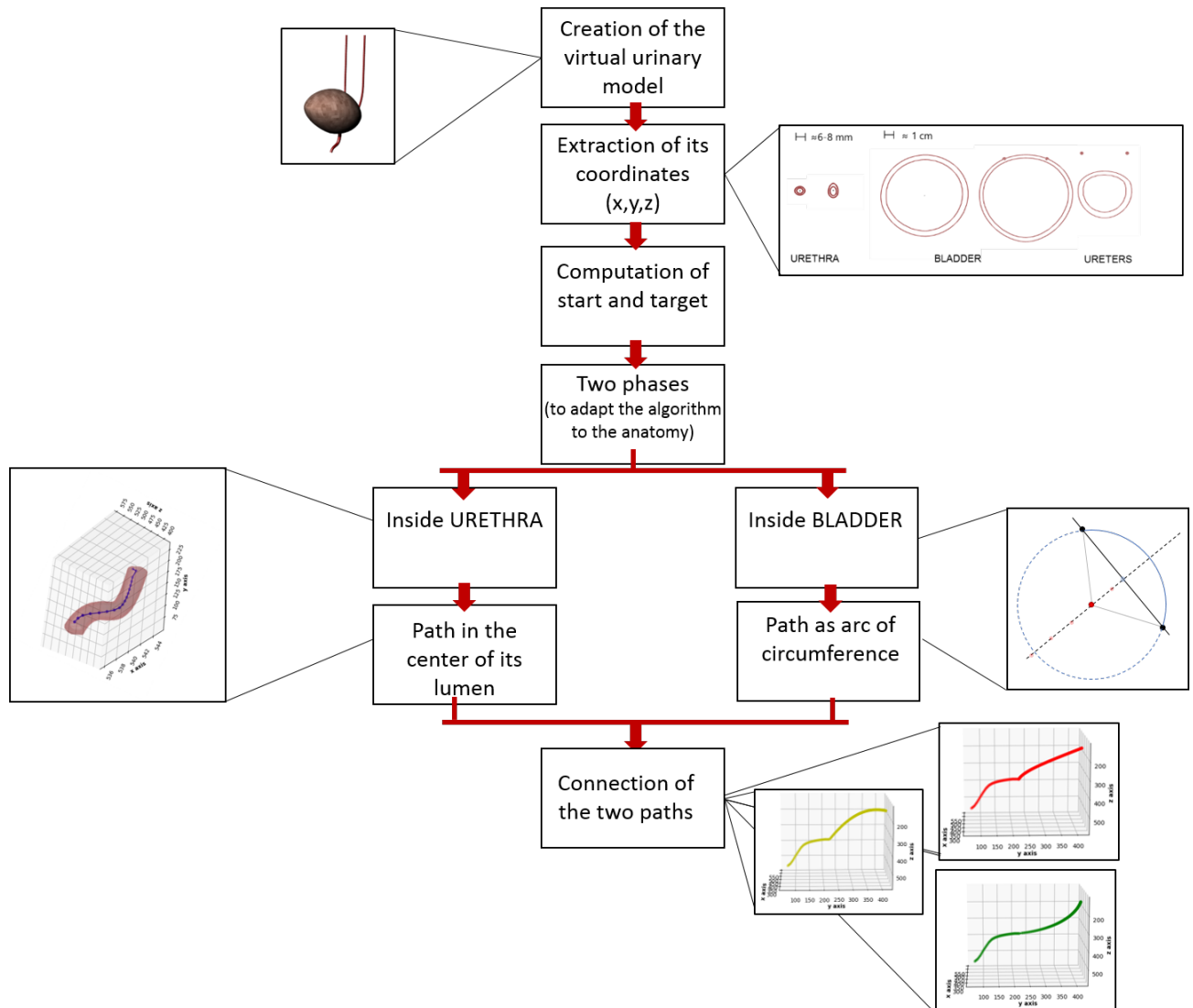

Figure 3.15: Flow chart of the main steps of the path planning strategy.

The first thing done was reconstructing the bladder model to extract the coordinate of the borders and create images of the sectioned model. Thanks to those images, the starting and the target point coordinates were computed.

Firstly, the OBJ file is loaded. As mentioned before, this OBJ file

contains vertex coordinates of the triangle meshes forming the model. Then, a plane perpendicular to x and z directions is created. They are, respectively, the frontal length and the width (or later length) of the bladder. The plane is constructed having as y coordinate the lowest y value present in the virtual model.

At this point, a loop scans every triangle present in the OBJ model and detect if it's above, below, or intersecting the current plane. If a triangle is being intersected by the plane, a line-plane intersection function [75] in the code will extract the coordinates of the two points, as shown in Figure 3.16. The coordinates of these points are then added to a list.
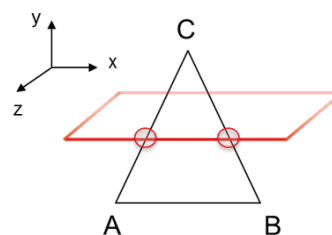

Figure 3.16: Visualization of how coordinates are get from OBJ triangular meshes with the line-plane intersection code.

The software is configured to repeat this sequence n times, each one with a new plane- always perpendicular to x and y, but each time incrementing the y value. The virtual model has a height of $\sim$10 cm and so the decision was to use n = 100 steps as to 'scan' the model every millimeter.

A visual representation of this step can be seen in Figure 3.17a. Each of the n times a new plane is created, the model is being intersected at a different y level, to retrieve all of the model coordinates.

Each time, the points computed with the line-plane intersection function (which correspond to the model x and y coordinates at a certain y value) are scaled to be drawn in an image. The final result will be n images displaying the border of the bladder for each of the y value adopted for the planes. An example of them can be seen in Fig. 3.17b. Thanks to the images drawn, the ureter orifices [Figure 3.18, right- one of which is the target of the path- can be computed. The start
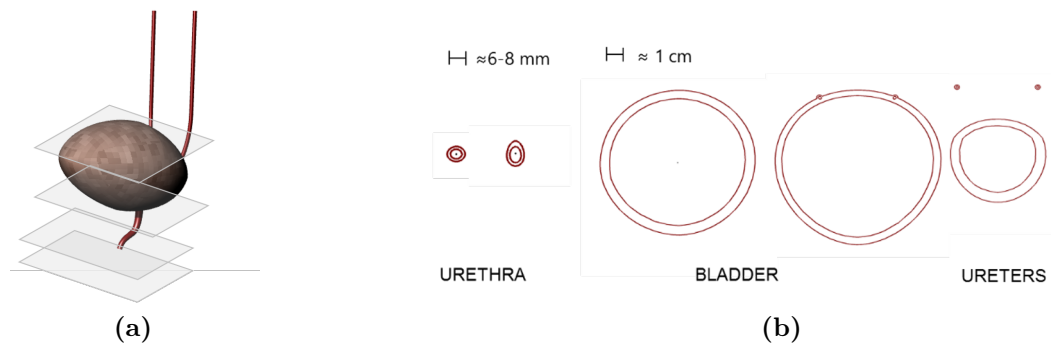
Figure 3.17: Visualization of how the model is sliced (a) and resulting printed images (b)

of the path, instead, is the central point (computed as the mean values of coordinates) in the lumen at the beginning of the urethra [Figure 3.18, left].
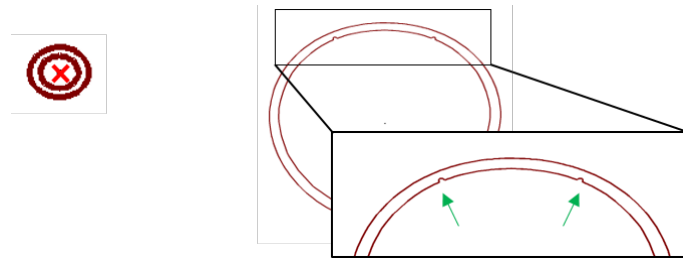

Figure 3.18: Starting (left) and target point (left) (one of the ureter orifices indicated with red arrows) of the path planning strategy.

To develop the optimal path to reach the ureter orifice, which is the target, the algorithm is implemented in two phases. One when the instrument is in the urethra and one from when it enters the bladder. This is done to optimize the strategy depending both on the prototype and anatomy characteristics.
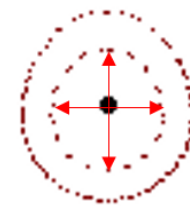

Figure 3.19: Section of the model in correspondence of the urethra in XZ plane.

Therefore, the first thing done was to divide the retrieved coordinates of the virtual model between those of the urethra and those of the bladder. When it is sectioned in y-direction, the urethra appears almost like a circle (see Fig. 3.19). Therefore, **distance**

between the center of the lumen and the borders in each image in x and z direction are computed [see red arrows in Fig. 3.19] in each of the image drawn at the previous step. If both values are below a certain threshold (~ 20 mm), at that y level the instrument is still in the urethra. When the values detected overcome the threshold it means the device, at that level, has entered the bladder.

As the strategy for when the device is in the urethra and for when it has entered the bladder are different, they will be explained in the next two different subsections.
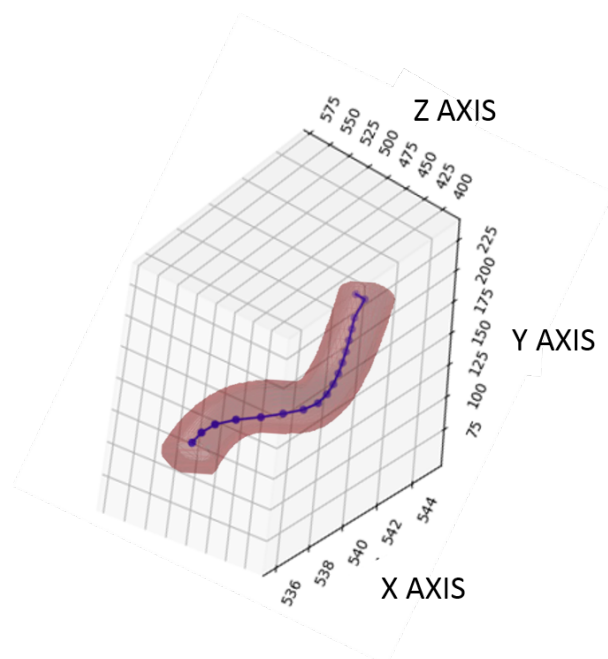
3.3.1   Inside urethra

Figure 3.20: Visualization of urethra model superimposed to the path made.

As the urethra is thin, the prototype doesn't have any range of movement. During the standard procedure, the surgeon pushes the instrument along the lumen. Depending on the haptic feedback that is received from the instrument, the medical practioner can understand

which movement he has to do to insert more of the instrument. Practically, the device proceeds just because it's constantly in contact with the walls and keep going. As the prototype doesn't have any force or pressure sensor, this strategy didn't seem appropriate as pushing without feedbacks would probably cause injuries to the lumen walls. The strategy adopted was to make the prototype proceed along the urethra staying in the center of the lumen, to avoid as much as possible any contact with its thin walls. The mean point in x and z directions were then calculated for each y level, starting from the lowest point of the urethra till its end – which corresponds to the bladder entrance.

3.3.2   Inside the bladder

Once the instrument has entered the bladder, it has more space of movement. As the bladder is made of soft tissue it may undergo deformation and its exact shape cannot be predicted in advance. To avoid as much as possible any unwanted obstacles (i.e. deformation of the walls of the bladder due to gravity) the choice was to develop few possible paths and then choose the optimal one and make the proper corrections based on mechanical and physical constraints, both of the instrument and the real environment. The

Figure 3.21: Section of a bladder in the frontal plane- The red point indicates the end of the urethra, while the green point indicates the ureter orifice. They correspond to the start and the target of the part of path planning when the device enters the bladder.

idea for the path strategy was given from Y. Zhao et. al. [62], whose strategy tries as a first attempt to connect the start and the target with a straight line. If no obstacles are encountered, the path is achieved. If obstacles are on the path, some curvatures are introduced to avoid
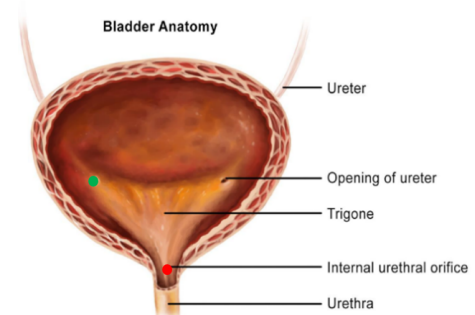
them. Their strategy was made for a known environment. As in this case the workspace - and so its obstacles - isn't predictable, the idea was to connect the start and the target with an arc of circumference. This choice was found as an optimal one as a steerable segment can easily follow a circular path. The arc of the circumference is designed in two dimensions. Therefore, the path is first designed for two coordinates. The third coordinate is then added spacing from the coordinate value of the start to the coordinate value of the target. The subsequent explained steps are performed in 3 different planes (plane XY, plane YZ, plane XZ).

Firstly, the coordinate of the start - entering of the bladder - and target -UO- points are computed [Fig. 3.21 and 3.22a]. Subsequently, the line connecting the two points (r) [Fig. 3.22b] and its mean point (M) [Fig. 3.22c] are computed. Then, the line (s) perpendicular to r and passing through M is computed [Fig. 3.22d]. Equations used to calculate the slope and the intercept of the two lines can be found below. In the equations m and $m_\perp$ are slopes of lines r and s respectively, while q and $q_\perp$ are the intercepts. x_S and y_S are the starting point coordinates. x_T and y_T are the target point coordinate. x_M and y_M are the mean point coordinates.

$$m = (y_S - y_T)/(x_S - x_T)$$

$$q = (x_S * y_T - x_T * y_S)/(x_S - x_T)$$

$$m_\perp = -1/m$$

$$q_\perp = y_M - m_\perp * x_M$$

On s [Fig. 3.22e], five points will be defined as the centers of the circumferences [Fig. 3.22d]. The points are chosen starting from M [Fig. 3.22c], on s [3.22d]. Each has a distance from the previous one ~13 mm in horizontal.
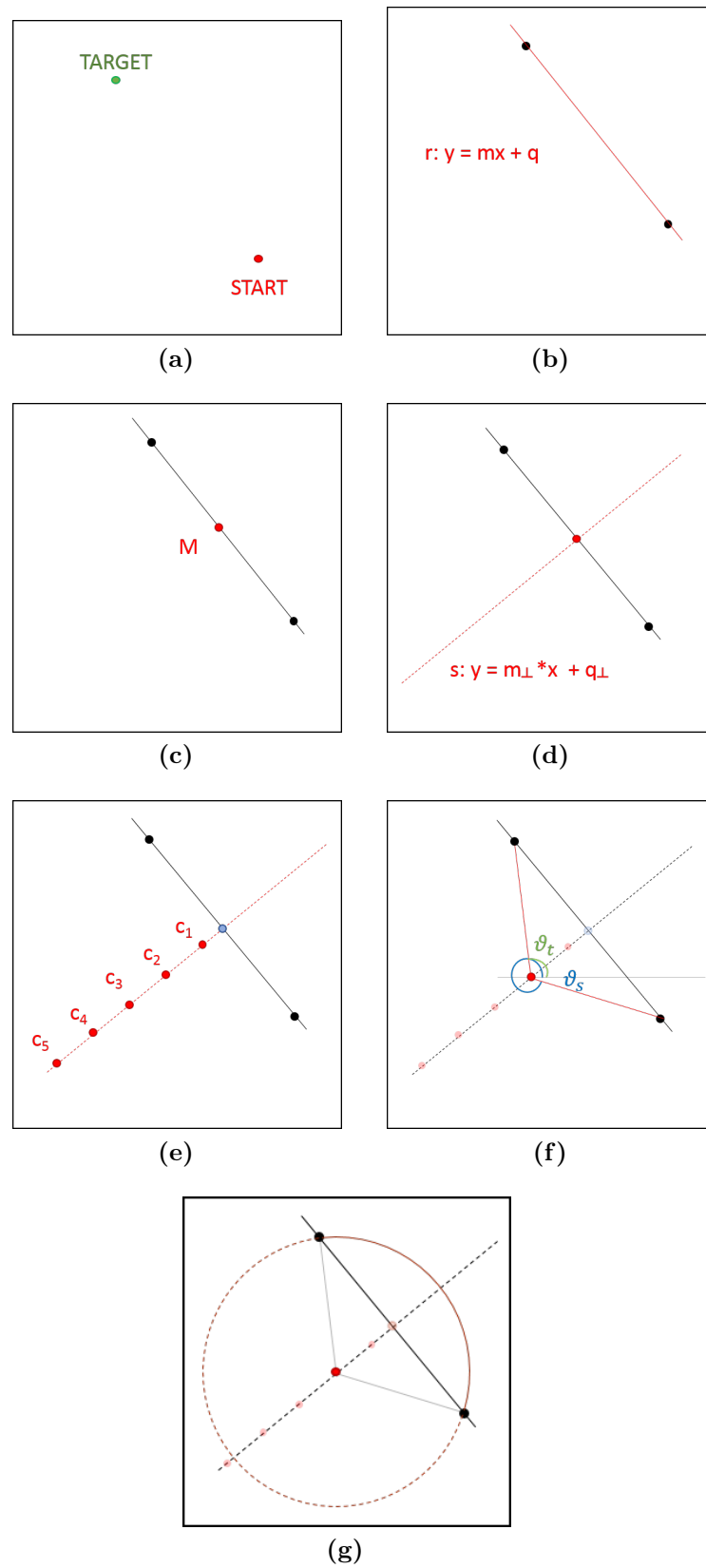
Figure 3.22: Visualization step-by-step of how the algorithm creates the 2D path in the bladder.

The next steps are performed for each of the points appointed as centers [Fig. 3.22d]. The radius of the arc of the circumference is calculated as the distance between the center and the starting point.

Then, the angles that the start (ϑ_S) and the target (ϑ_T) forms with the center are calculated with the formulas 3.2, where x_C and y_C are the center of circumference coordinates and r is its radius [Fig. 3.22f].

$$\vartheta_S = 2 * arctan((y_S - y_C)/(x_S - x_C + r))$$
$$\vartheta_T = 2 * arctan((y_T - y_C)/(x_T - y_C + r))$$

(3.2)

Then, an arc of circumference is calculated between the start and the target points. The coordinates of the arc of circumference forming the path are calculated thanks to a loop, as described in formula 3.3, where x_P and y_P are each generic point coordinates and ϑ is the angle formed by that point [Fig. 3.22g]. At each step in the loop, the angle (ϑ) is incremented of 1 degree, in order to compute all the coordinates of the path between the start and the target points.

$$x_P = x_C + r * cos(\vartheta)$$
$$y_P = y_C + r * sin(\vartheta)$$

(3.3)
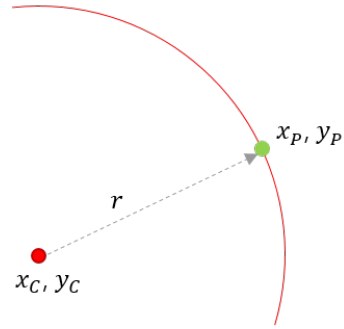
Once the arc of the circumference is defined, the third coordinate is added. This has been done spacing from the target to the starting value. At this point, for each plane (XY, YZ, XZ) , 5 paths were available. In total 15 possible paths are available to proceed into the bladder. The paths created – for the permanence of the device in the

urethra and the one in the bladder- are then connected. Three examples – one for each of the different planes in which 2D circumference was firstly created – can be seen in Figure 3.23.

At this point, each path had to be checked twice before being considered usable. First, it was checked that the path coordinates don't collide with the model bladder walls. This would mean performing a path outside of the region of interest and – in a real environment - a possible injury to the anatomic structure. A second check was performed to consider the kinematic threshold of the device. For the way the path is designed, there are no sudden change of directions and the trajectory appears to be smooth. The radius of curvature of the prototype couldn't overcome 20 mm. To be sure that this was respected, the path
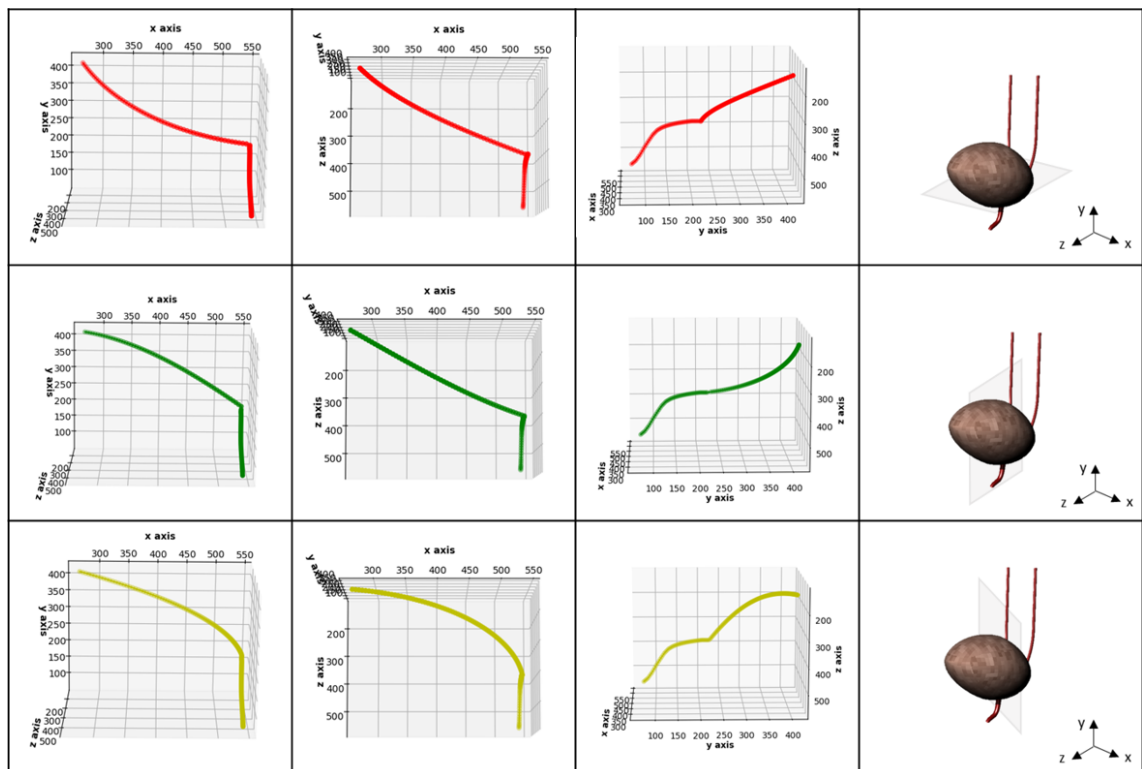

Figure 3.23: Path planning strategy in the three planes in which the 2D circumference has been developed. The red one is when the circumference is created in XZ plane, the green one in YZ plane and the yellow one in the YX plane. In the same row a visualization of the bladder and the plane in which the circumference is created. They will be called respectively path 1, path 2 and path 3.

was checked to see that the angles performed along its segments were compatible with the mechanical properties of the instrument. To do that, the angle formed between three adjacent points (corresponding to start, mid and end point of a segment prototype) is calculated. First, the segment formed between the first two points (A and B) and the one formed between the last two (B and C) are calculated [3.24]. Then, the angle in between is calculated. The limit value (120°) was chosen once the prototype was printed and seen its mechanical limit in a real environment. The solutions obtained with the circumference created in the XZ plane – 3.23 (first row) – seem to be suboptimal for two main reasons. The first one, as can be seen in Figure 3.23 (first row) and 3.25, is that the path runs close to the border of the bladder.
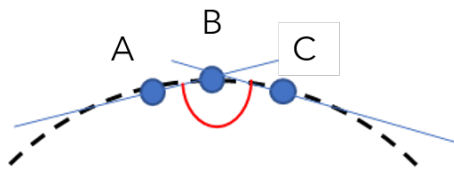

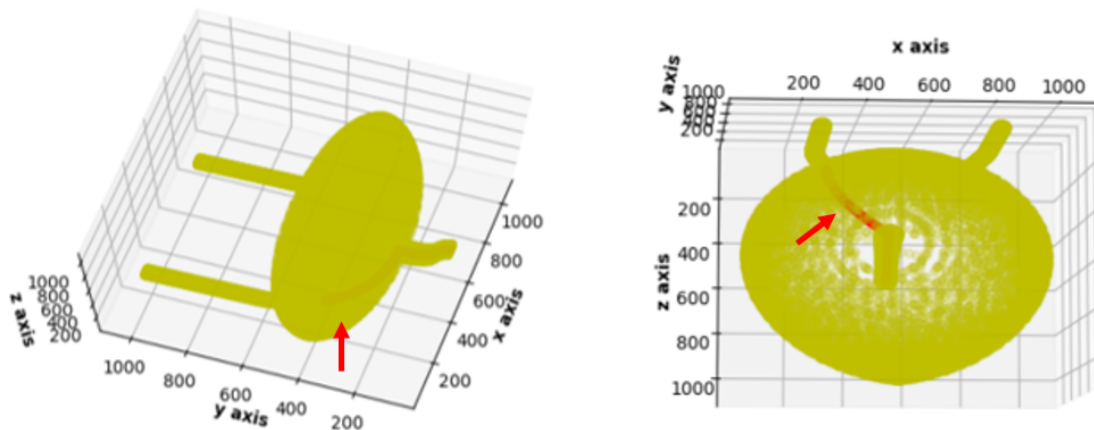**Figure 3.24:** Visualization of how the max deflection angle is calculated.

Figure 3.25: Visualization of path 1 and bladder model.

This could be a problem as the bladder walls could undergo deformation (i.e. due to gravity) and not be in the expected position. This could lead to an unwanted collision between the device and the wall. The other

reason is that the direction of the entrance of the UO seems inadequate. In a robotized device this could cause problems during the entrance or the need for additional maneuvers by the surgeon to correct the direction of the entrance. The other two paths (2 and 3) seem preferable. They are both far from the bladder walls and the direction of entrance seems more appropriate.

Regarding the entrance direction, the green path [Figure 3.23] seems the optimal one as it has a perfect direction of entrance as it is perpendicular to the bladder wall close to the orifice. Even though this is the best choice, the both green and the yellow paths can be chosen as the prefered ones, as, in the case for example a predictable obstacle (i.e. cancer formation, as can be seen in Fig. 3.26a, where a cancer formation is simulated in the model) would interfere with one path, the other could be used .
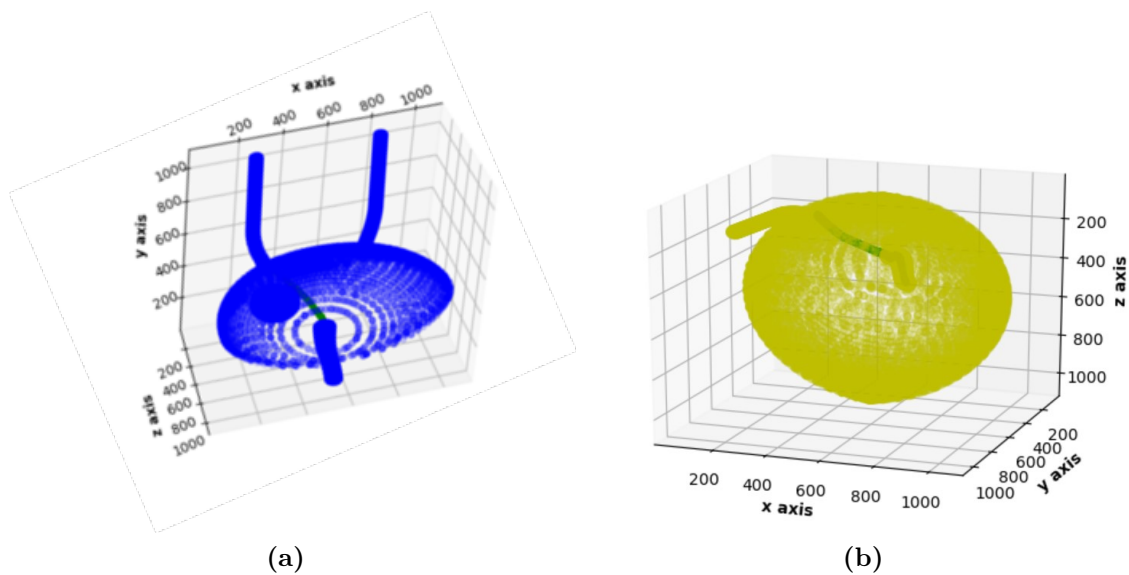

(a)   (b)

Figure 3.26: Path 2 in presence of an obstacle (a) and visualization of its entrance of direction (b).

4

Experimental Activities

4.1 Experimental setting

This section will describe how the phantom models were made, enhance EM tracking principles, and the final setup of the experiments.

4.1.1 Phantom bladder & urethra model

To create the bladder model, two negatives of the molds [Figure 4.1a, 4.1b] based on the model made in Rhino®, were 3D printed. The printer used is Ultimaker 3 [76] and the material is PLA (Polylactic acid). Subsequently, the silicon rubber was poured in them. The silicon rubber used was PS 85-10, pink-colored. A balloon is inflated and put between the two negatives before pouring the mixture to have a model empty inside. The urethra has been done separately and subsequently attached with superglue. Similarly as done for the bladder, a mold for the urethra lumen has been 3D printed [Fig. 4.1c] and then silicone has been poured in it. This way, the model would have a lumen of realistic dimensions and also compatible with the prototype diameter. The resultant model
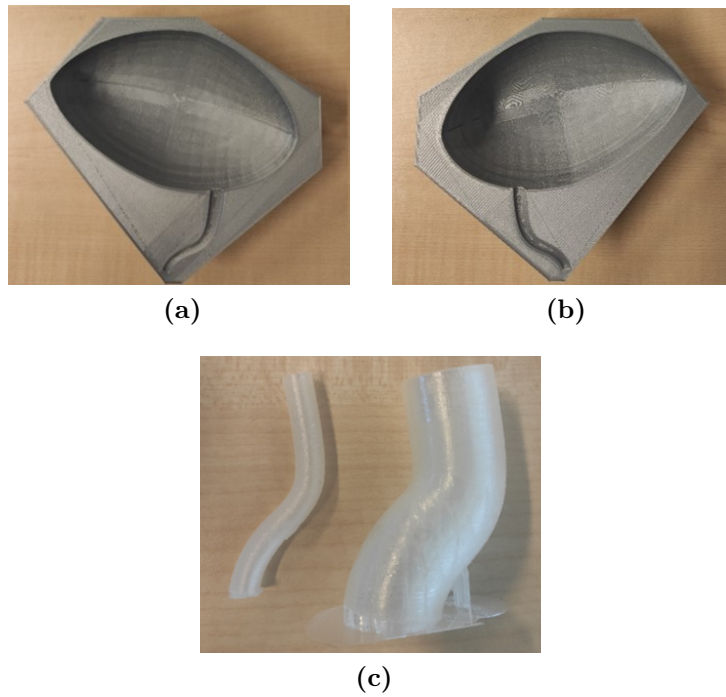
can be seen in Figure 4.2.

(a) **(b)**

(c)

Figure 4.1: Molds for the bladder (a & b) and the urethra (c).
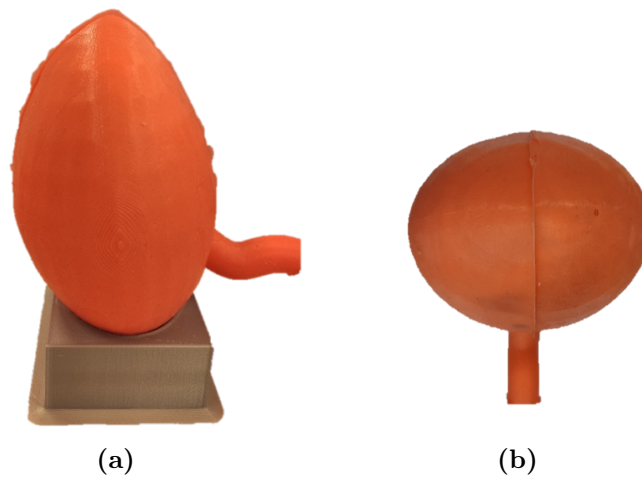

(a) **(b)**

Figure 4.2: Side (a) and top (b) view of the bladder model on its custom designed support.

4.1.2 Electromagnetic tracking

The tracking of the prototype tip for the validation of the path computed has been realized thanks to Electromagnetic (EM) tracking.

More information relative to EM tracking principles and functioning can be found in the Appendix.
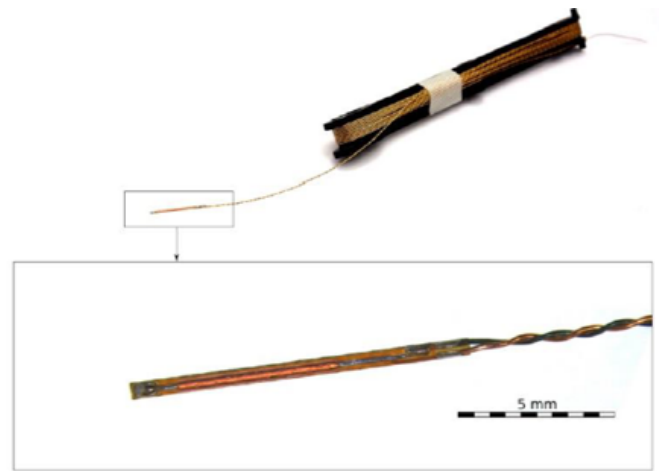

Figure 4.3: Aurora ® 5DOFs sensor.

For our application, Medical Aurora® V3 from Northen Digital Inc (NDI) was used [77]. Its main components are the planar field, the System Control Unit (SCU), the sensor interface unit, sensors, and tools. Data are gained with the software provided by NDI and subsequently processed. The maximum refresh rate available of the instrument is 40 Hz). The system was used in the cube volume configuration (working volume: 500 mm^3) [Figure 4.5]. Moreover, in our application no particular ferromagnetic devices or instrumentation which could distort the magnetic field was present. Therefore, the system was proved to be robust against environment. The sensor used for tracking is the Aurora® 5 DOF sensor (Part No. 610090) [78] [see Figure 4.3]. The sensor was placed inside the hollow grooves of the prototype.
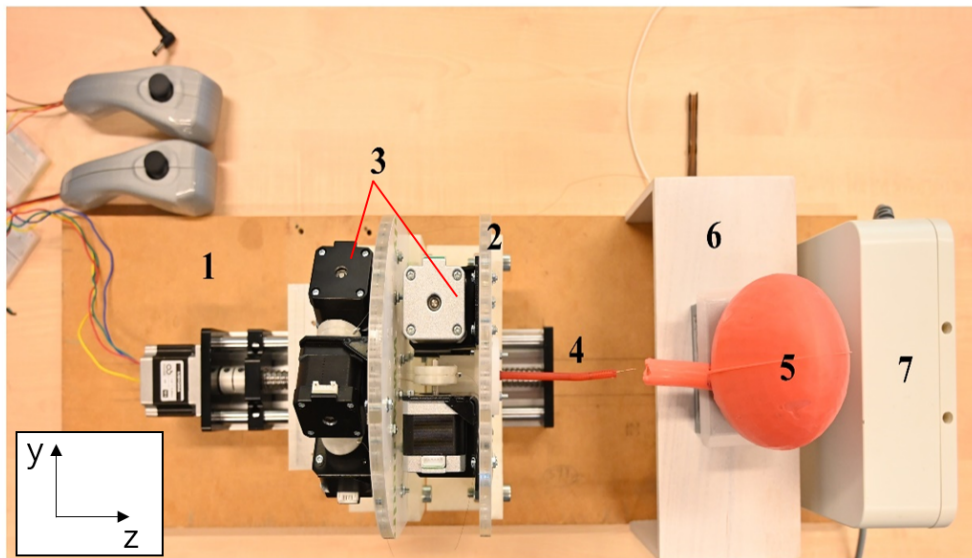
4.1.3 Final setup

In Figure 4.4 the main components of the experiments set up can be seen: Aurora® field generator (7), a linear slide (1), supports for the prototype (2), stepper motors controlling prototype segments (3), the

prototype (4), the bladder model (5), and its support (6).
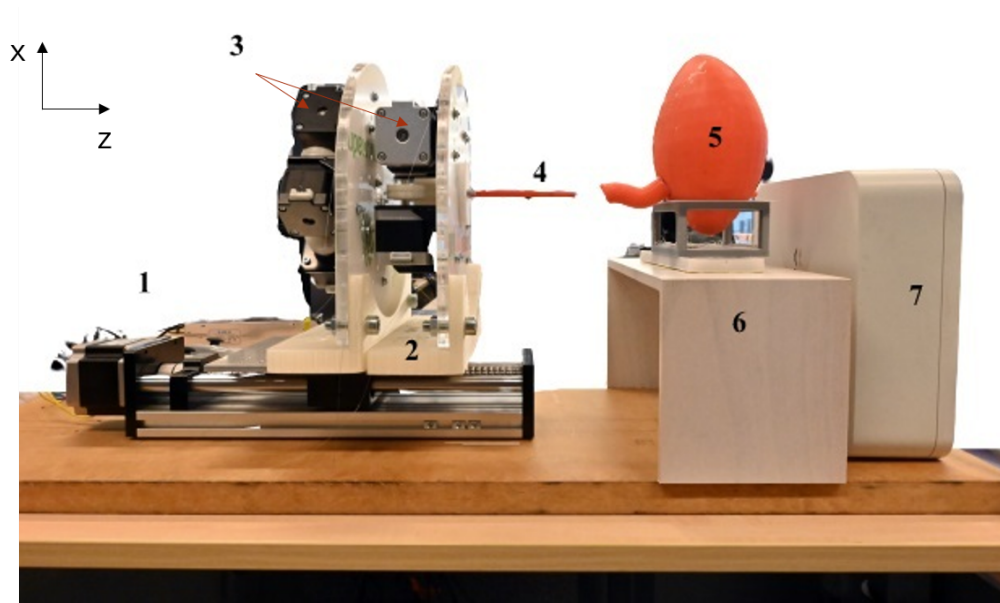
(a)

(b)

Figure 4.4: Side (a) and top (b) view of the setup. In the photos are visible: the linear slide (1), the prototype support (2), stepper motors (3), the prototype (4), the phantom bladder model (5), model support (6), and Aurora® field generator (7).

Aurora® SCU and Sensor Interface Unit (Fig. 4.6) are located close to the host computer, more than 1 m apart from the field generator, as needed to avoid interference with the magnetic field. The field generator

and the slide are mounted and sewed to a wood platform. This way no relative motion between the two components could occur and accuracy and errors would remain constant during different days and trials. The slide was mounted at ∼20 cm from the field generator. This was chosen as the working space of the EM tracker starts at 5 cm far from the field generator border [see Figure 4.5].
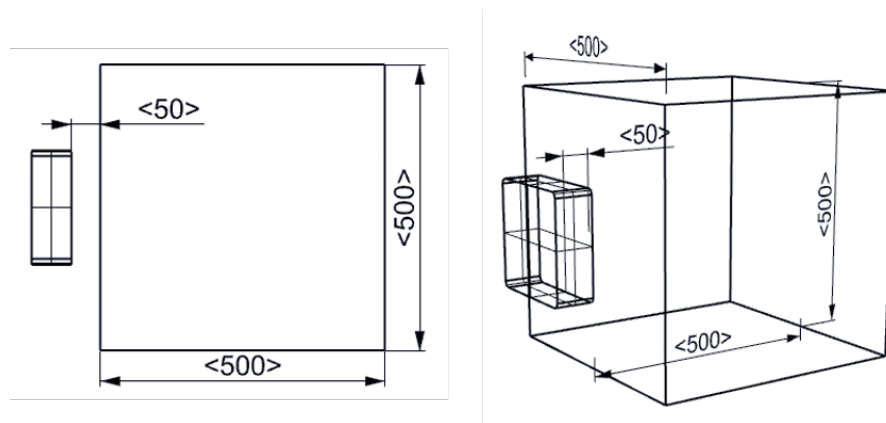

Figure 4.5: Top (left) and side (right) view of Aurora® field generator and corresponding cubic working space. Scale is millimetric.

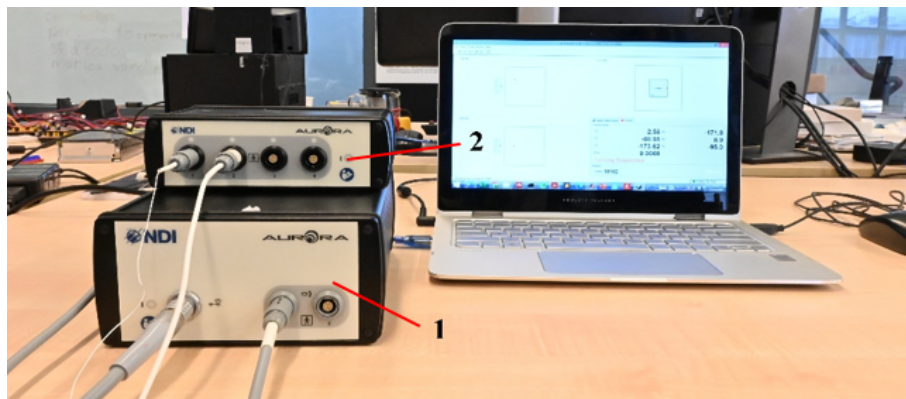**Figure 4.6:** Aurora® SCU (1), Sensor Interface Unit (2) and host computer.

A platform supporting the prototype is mounted on the linear slide. The slide is connected to and actuated by a stepper motor. It is controlled by the two joystick buttons, which make the slide move in z-direction when being pressed [see Figure 4.4. One joystick makes the slide go forward, the other makes the slide go back. The joysticks control also

the prototype movement in x- and y-directions [see Figure 4.4. Each joystick controls four stepper motors which make the segments of the prototype move in four directions (up, down, left, right). Therefore, thanks to the slide and the joysticks the prototype can be steered in three directions. A schematic of cables connections can be seen in Figure 4.7.

Figure 4.7: Schematic of Arduino connections.
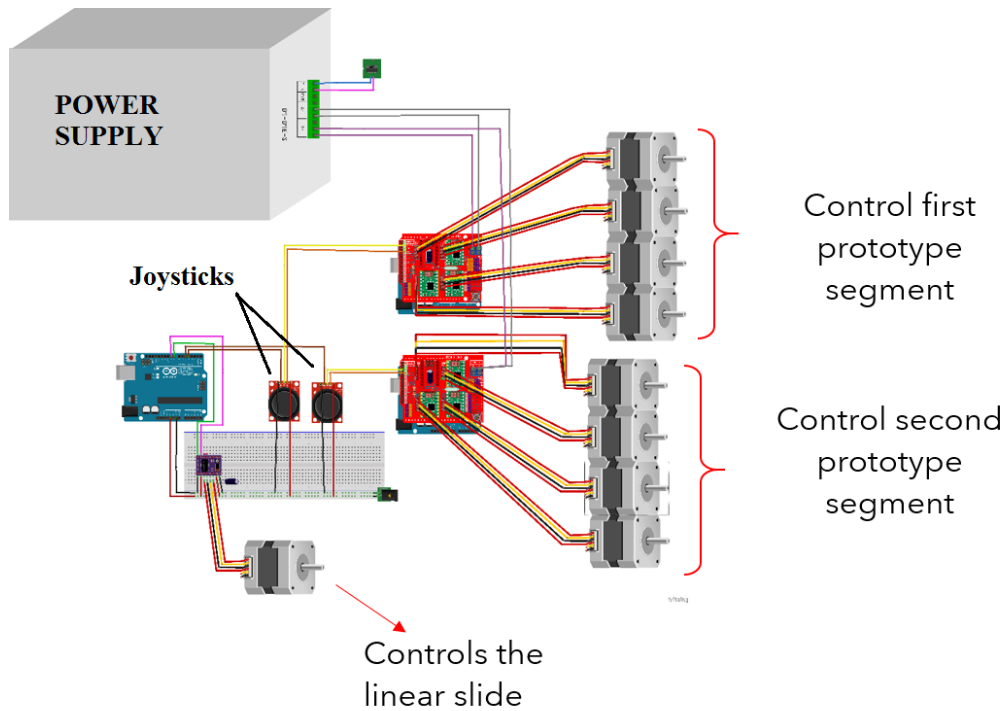
In total, three Arduino®Uno boards were used, one for the control of the slide and one for the control of each segment. To record the movements of the tip of the prototype, the Aurora® 5 DOFs sensor is inserted in the tip of the prototype. A close-up picture can be seen in Figure 4.8.
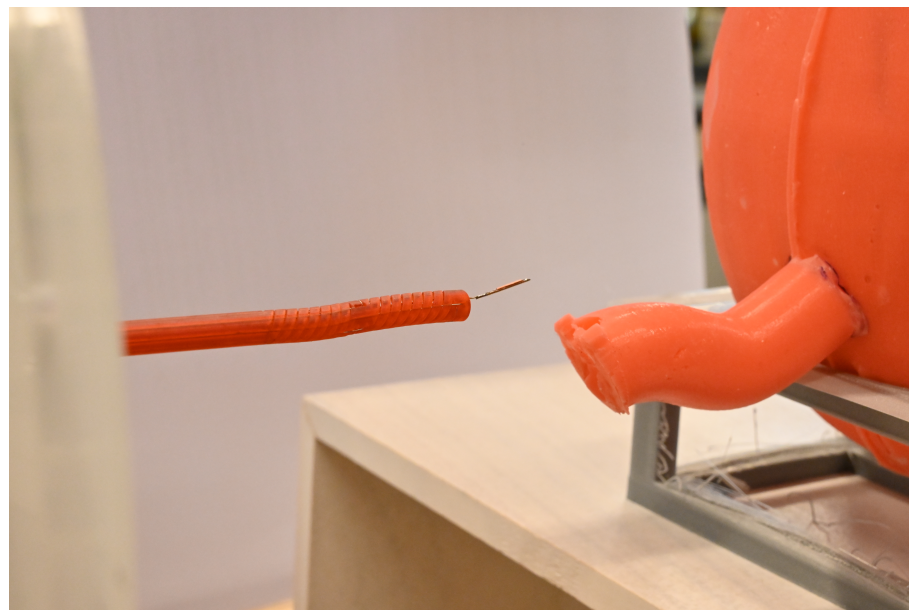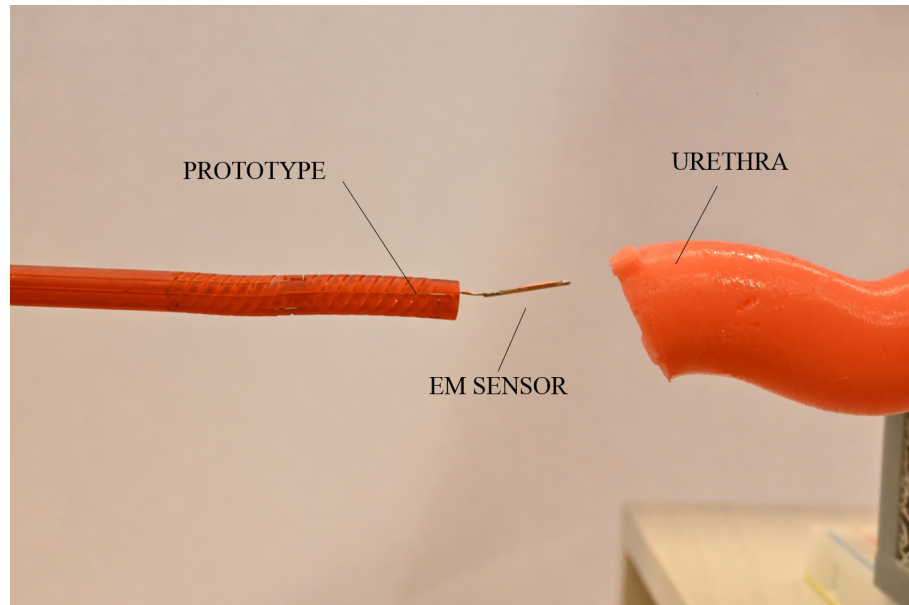
PROTOTYPE

URETHRA

EM SENSOR

Figure 4.8: Close up of prototype tip, sensor, and phantom model.

4.2   Experimental protocol

To validate the path and the prototype design, few experiments have been conducted. The choice of those was made to see:

1. if the prototype mechanical limits were correct for its steering in a phantom urinary model;

2. if human control could easily guide the prototype and follow the path;

3. if the path was able to make the participants guide the prototype toward the target;

4. if feedback received from the optimal path were important for improvements in time and precision.

Two different modes of experiment have been conducted. The goal of both the experiments was for participants to control the prototype and guide its tip towards the target, set as one of the orifices of the model. Both silicon model orifices have been set as targets. The same silicon phantom (bladder and urethra) is used for all the trials. Three different subjects have been asked to perform the trials. Before starting, they spent around 10 minutes practicing to get familiar with the joysticks and tip steering.

For each orifice (right and left) of the model, six trials have been performed. The first 3 trials (**mode A - voice guidance group**, Fig. 4.9a) were performed by the participant moving the prototype following directions given by another user. The latter one was an external subject who could see inside the bladder (from a hole created in the silicon model) and could then give directions to guide the participant to move the prototype toward the target (= orifice of the phantom model). The last 3

trials (**mode B – visual guidance group**, Fig. 4.9b) were performed by the participant just following the optimal path as a reference, without anyone's instruction, trying to reach the target. This was possible using and modifying the Python interface for Aurora®: *scikit-surgerynditracked* ([79] Copyright ©2018, University College London All rights reserved). Thanks to the code, when performing experiments in mode B, the recorded data were displayed in real-time on the screen, where they could superimpose the optimal path.

(a) Mode A - voice guidance group
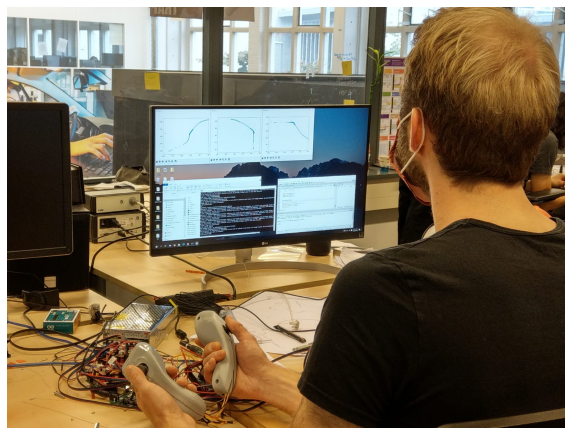
(b) Mode B - visual guidance group

Figure 4.9: One of the participants while performing the two modes of the experiment

4.2.1 Quantities measured

Those tests were performed to record the subsequent quantities. In all performances, the tip position during the trial, its final position and time duration are recorded. Each time the EM tracking recording system was set at 180 seconds, with a frequency equal to 1 Hz. The recording was stopped before when the target was reached. In all trials of mode A, Aurora® needle (pt. 610062, [80]) was used as a reference and positioned on the bladder model support, while for trials of mode B the internal reference system was used.

4.2.2 Experiments performance indicators

The final position of the prototype in the bladder model was analyzed, to see if the prototype could reach the target. Success would be encountered if the prototype would be able reach the target or its proximity (1 cm^2 around it). In mode A (voice guidance group) this would mean the prototype can steer in a urinary phantom model. In mode B (visual guidance group), this would mean the only support of the path can guide the participants in reaching the target. The position of the tip of the prototype was recorded, exploiting EM tracking. The paths, reconstructed from the positions recorded, have been plotted to have a visual comparison between the different modes (voice and visual guidance group).

The time necessary to complete each trial has been recorded, to investigate if a learning curve would be present as more experiments were performed.

The lengths of the path have been calculated and evaluated with a Student T-Test to see if a significant statistical difference was present

between the two modes (voice and visual guidance group).

Participants have also been asked to share their comments to understand how to improve the user experience and to evaluate the easiness of manual control.

4.2.3 Data analysis

The recorded data have been filtered in MATLAB with a **locally weighted regression filter (LOWESS)** to filter out the noise. It automatically reconstruct a linear regression weight function for the data points contained within the span. The span data parameter used was 20%, which, considering the high refresh rate and the slow movement of the prototype, has been considered as the right choice. The local regression smoothing process follows these steps for each data point:

- Compute the regression weights for each data point in the span. The weights are given by the tricube function shown below.

$$w_i = (1 - \left| \frac{x - x_i}{d(x)} \right|^3)^3 \qquad (4.1)$$

In eq. 4.1, x is the predictor value associated with the response value to be smoothed, x_i are the nearest neighbors of x as defined by the span, and $d(x)$ is the distance along the abscissa from x to the most distant predictor value within the span. The weights have these characteristics:

-The data point to be smoothed has the largest weight and the most influence on the fit.

-Data points outside the span have zero weight and no influence on the fit.

- A weighted linear least-squares regression is performed. The regression uses a first degree polynomial.

- The smoothed value is given by the weighted regression at the predictor value of interest.

Used in [81] by E. Pouline et. al. and stated to be one of the best choices by Qi et. al. [82], this filter appeared as the best solution for our application. This filter works fitting simple models to localized subsets of the data to build up a function that describes the deterministic part of the variation in the data, point by point. One of the greatest attractions of this method is, in fact, that the data analyst is **not required to specify a global function** of any form to fit a model to the data but only to fit segments of the data.

Before performing experiments to validate the path, a trial was made to check if any systematic error was present in the recordings. The sensor was attached to the prototype support. The slide motor has been set to run the platform along the slide for 12 cm. Therefore, the only direction along which the sensor is moved is z. The support starting point was close to the field generator and the movement brought it farther. Samples were recorded for 20 seconds at a rate of 40 Hz. The reference system used was the one internal to the Aurora® field generator. The accuracy of recorded data in z-direction was calculated using the Root Mean Square Error (RMSE) formula 4.2, and resulted higher than 98%.

$$RMSE = \sqrt{(\frac{1}{n}) \sum_{i=1}^{n} (y_i - x_i)^2} \qquad (4.2)$$

The total length travel recorded was, in fact, only 1.8 mm above the real value. Some oscillation [see Figure 4.11a, 4.11b, 4.11c, 4.11d] around the mean value can be seen both in x and y directions. These are of the

56

order of ± 2.4 and ± 1 mm for x and y direction respectively. They were expected as the slide is spiral-like [see Figure 4.10] and the platform oscillates accordingly. Even if the slide contains some metal parts, it was


**Figure 4.10:** Linear slide with spiral-like central rail.

seen that no interference with the magnetic field occurred. The motor used for the motion of the slide and the slide itself are not meant for clinical use. They were used as in this validation the accuracy needed in operating rooms is not required. The LOWESS filter was applied to data. In Figure 4.11b blue points are real data, red ones are filtered data. At this point in y- and x- directions was seen a systematic trend. Both x and y values tend to decrease when the sensor is moving far from the magnetic source [see Figure 4.11c and 4.11d]. The linear regression line for the filtered data was found and some corrections were made to avoid this trend. The recorded data and the filtered and corrected data, in 3 dimensions, can be seen in Fig. 4.11e. As the result was satisfying, no more filters or corrections have been made.
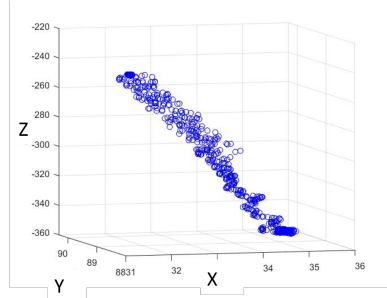
(a) Data recorded with the EM tracker in a 3D plot. Axis span are not equalized, scale is millimetric.
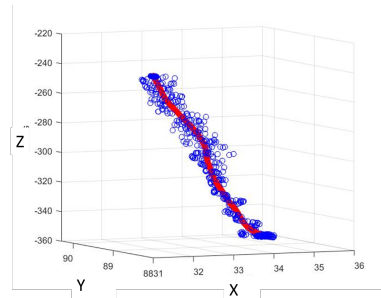
(b) Data recorded with the EM tracker (blue points) and data after local regression filtering (red points).Axis span are not equalized, scale is millimetric.
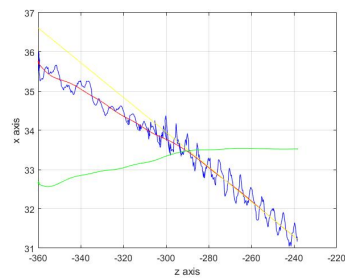
(c) Z-Y trend of recorded data (blue), filtered data (red), linear regression line (yellow) and data after linear correction (green). Scale is millimetric.
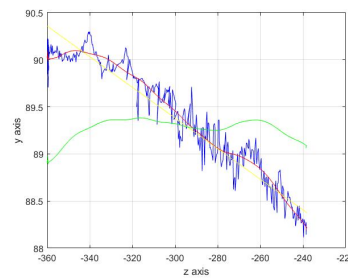
(d) Z-X trend of recorded data (blue), filtered data (red), linear regression line (yellow) and data after linear correction (green). Scale is millimetric.
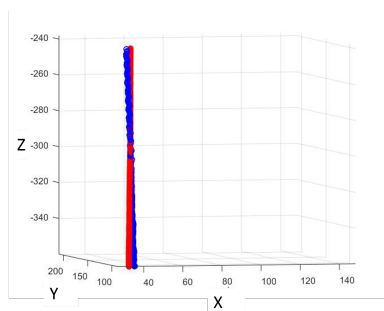
(e) 3D representation of real data (blue) and data after filtering and correction (red). Axis span equalized, scale is millimetric.

Figure 4.11: Recorded data analyzed with MATLAB.

5

Results & Discussion

5.1 Results

In both groups (with and without the visual aid) the users could control the segments and steer the prototype inside the bladder.

In all trials, in the **voice guidance group**, the target (or its proximity – 0.5 cm around it) has been reached. During the trials of participant #1 the sensor was positioned outside of the tip. Due to its damage, it was decided to keep the sensor inside the tip for the rest of the experiments, even if this would mean offsetting the recording point by ∼1 cm of the end of the tip.

In the **visual guidance group**, the trial was terminated when the user thought it reached the orifice or when the total length of the shaft was inserted in the model. The users entered the bladder correctly but failed in reaching the exact point set as the target. In all trials, the final points reached were in a radius of 1 cm than the chosen target.

Figure 5.1 displays the **time (in seconds)** needed for the participants to reach the targets in the two different group of trials. Participants
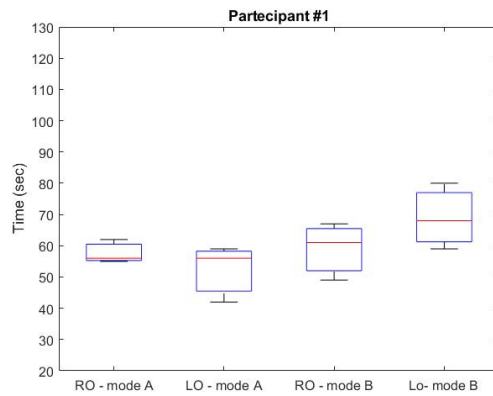
(a)
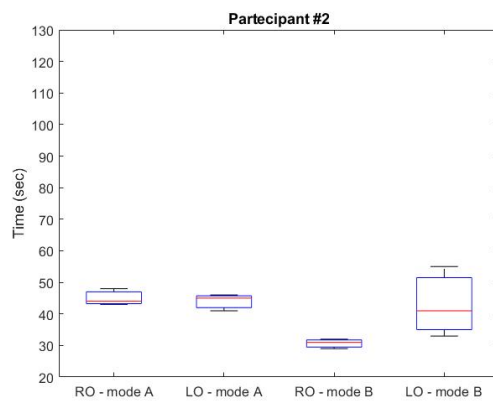
(b)
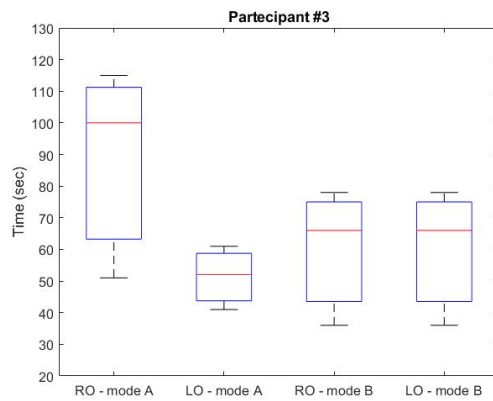
(c)

Figure 5.1: Boxplots of time (in seconds) each participant took to complete the trials. Mode A: voice guidance group. Mode B: visual guidance group. RO: Right Orifice set as target. LO: Left Orifice set as target. Mode A: Voice guidance group. Mode B: Visual guidance group.

#2 and #3 took less time in the last sets of trials, which is plausible as they felt more aware of the joystick control, while participant #1 took

more time in performing the trials with the visual support.

Moreover, it can be noted that the participants didn't follow the path in the urethra steering in 3 directions, but only proceeded moving forward. This led to the entrance in the bladder anyway, as the prototype is harder than the model and could deform it easily.

All the considerations stated can be seen in the **figures reportes in Tables 5.1 and 5.2**. The path could almost be followed in XZ (Top view) and ZY (Side view) planes but failed In XY (Front view) planes. This is since the path is modeled following the urethra anatomy, while the participants proceed moving forward without steering as their focus was on the screen with the Top view (XZ plane).

The length of each path during all trials was calculated. The results can be shown in Tables 5.2a, 5.2b, and 5.2c. As can be seen from the graphics in Fig. 5.2, the length of the paths when using the visual support was shorter.

The users were asked to give impressions regarding the setup. All participants felt easy and intuitive to control the tip movement and gained more awareness of it as moving on with the trials. The control exploiting joysticks has appeared to be ergonomic and user friendly. One stated that at the beginning the tip seemed to him/her too sensitive, but quickly understand the correct way to control it. The same participant felt intuitive that the right hand controlled the distal segment and the left hand the proximal one. Even if he/she could reach the target with the visual support, he/she preferred to be guided inside the trials, as having 3 screens to look at felt a bit confusing. On the contrary, another participant claimed to prefer the visual reference of the path instead of being given direction. He/She stated to prefer to look at the screen as the delay between the motion of the tip and its reference on the screen

was appropriate, while when being given directions, he/she couldn't understand how much steering was necessary.

Table 5.1: Top, side, and front view of the trials of the three participants reaching the Right Orifice. In **red** data collected with the **voice guidance group**, in **blue** data collected with the **visual guidance group**. In **black** the **path planning strategy**.**each row refer to a different participant (part #)**.

Part.	TOP VIEW (XZ)	SIDE VIEW (ZY)	FRONT VIEW (XY)
#1			
#2			
#3			
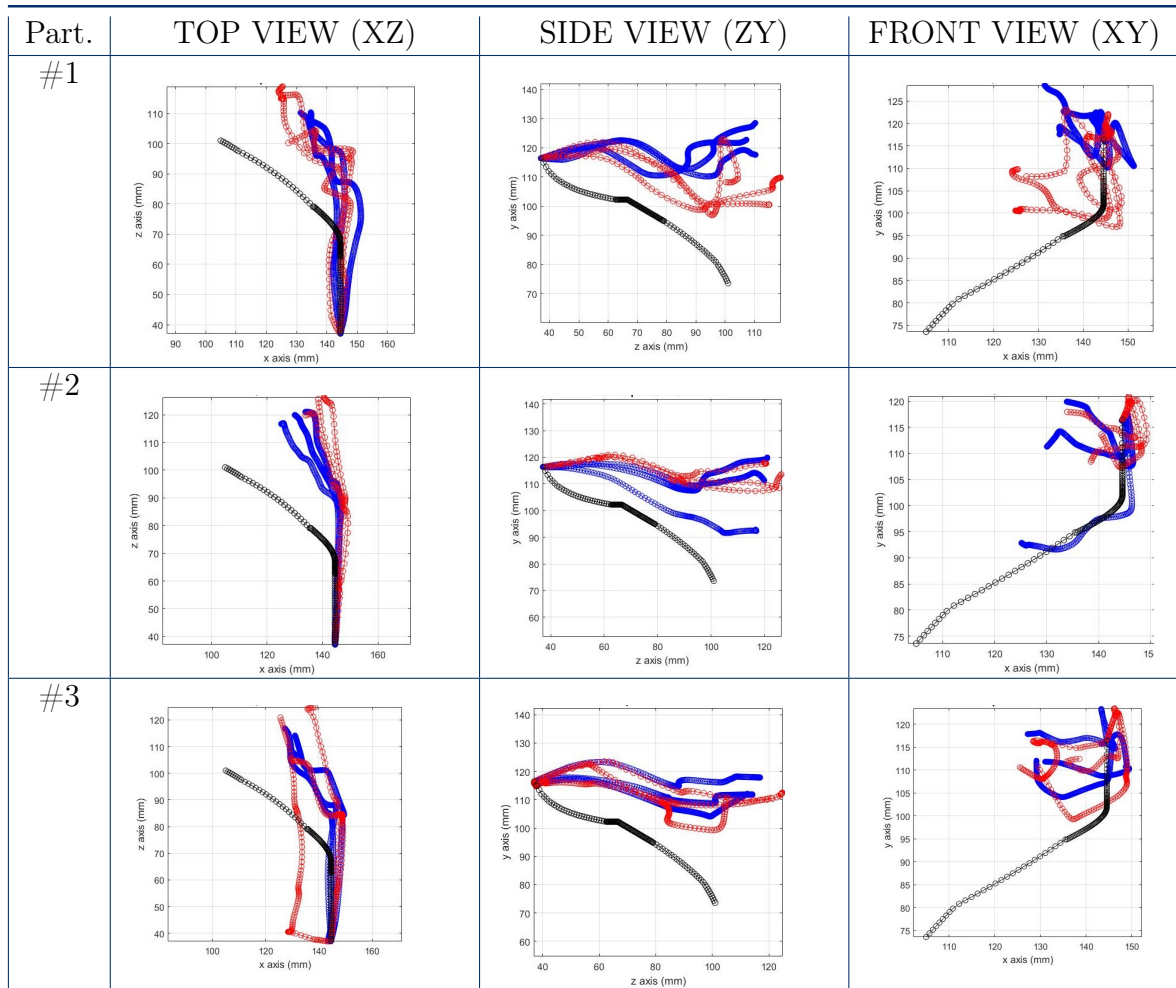
Table 5.2: Top, side, and front view of the trials of the three participants reaching the Left Orifice. In **red** data collected with the **voice guidance group**, in **blue** data collected with the **visual guidance group**. In **black** the **path planning strategy**. The trials refer to reaching the right orifice, **each row refer to a different participant (part #)**.
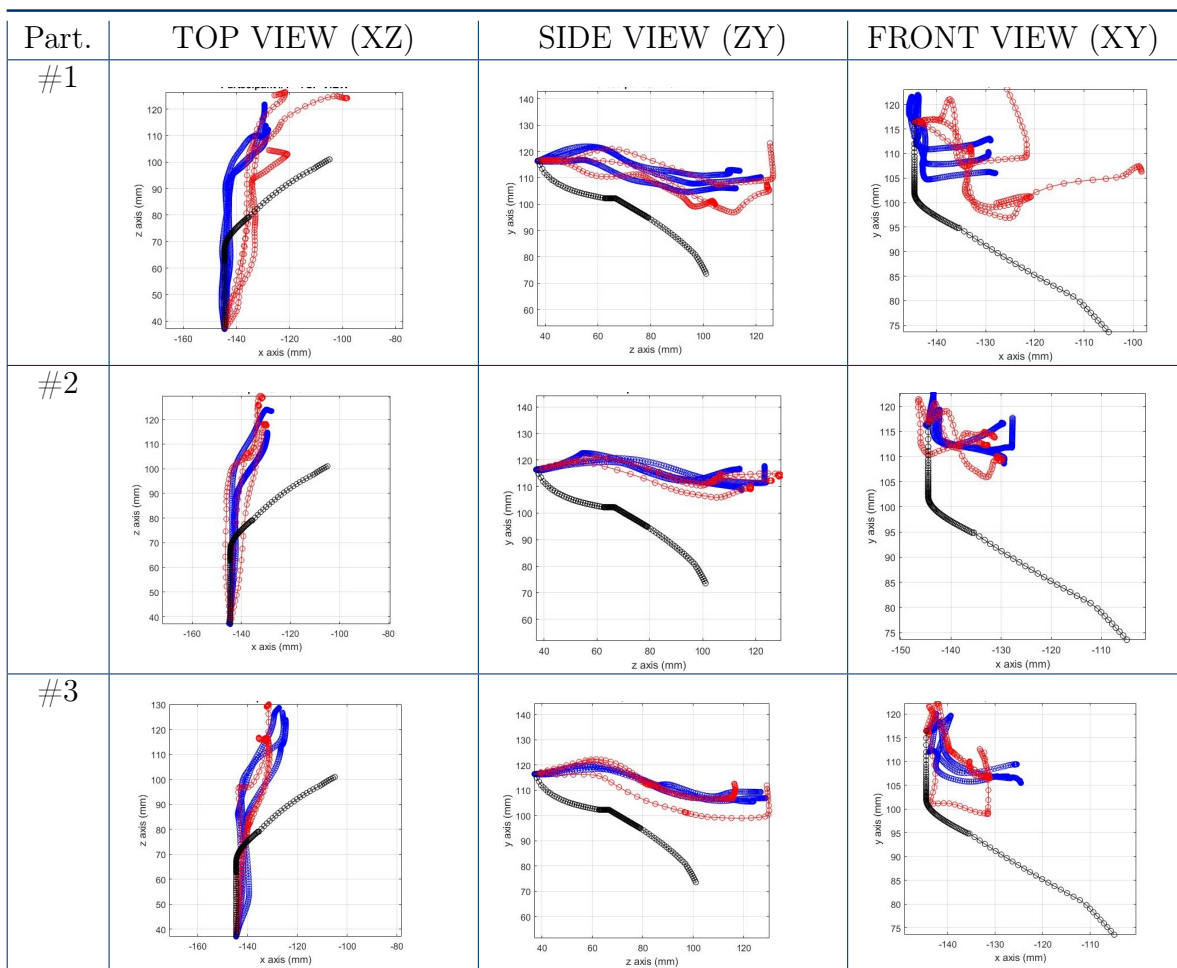
Part.	TOP VIEW (XZ)	SIDE VIEW (ZY)	FRONT VIEW (XY)
#1			
#2			
#3			

Table 5.3: Partecipant #1- lengths of the paths during the trials.

Part.1		
Trials	Mode A (mm)	Mode B (mm)
1	95,4	83,2
2	112,0	87,8
3	124,6	92,7
4	87,2	85,3
5	117,6	86,1
6	112,4	85,9
MEAN	108,2	86,8
STD DEV	12,9	2,9

Table 5.4: Partecipant #2- lengths of the paths during the trials.

Part.1		
Trials	Mode A (mm)	Mode B (mm)
1	88,5	84,7
2	97,7	82,7
3	100,5	99,8
4	93,3	89,5
5	96,5	93,8
6	91,2	93,3
MEAN	94,6	90,6
STD DEV	4,1	5,8

Table 5.5: Partecipant #3- lengths of the paths during the trials.

Part.3		
Trials	Mode A (mm)	Mode B (mm)
1	89,3	93,9
2	90,3	98,8
3	113,9	98,8
4	94,5	86,4
5	101,0	89,2
6	96,6	91,5
MEAN	97,6	93,1
STD DEV	8,3	4,6

(a)

(b)

(c)
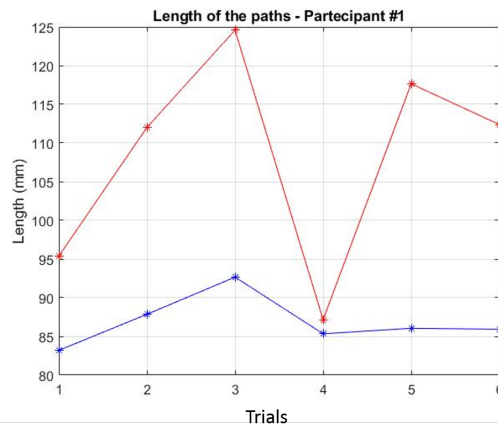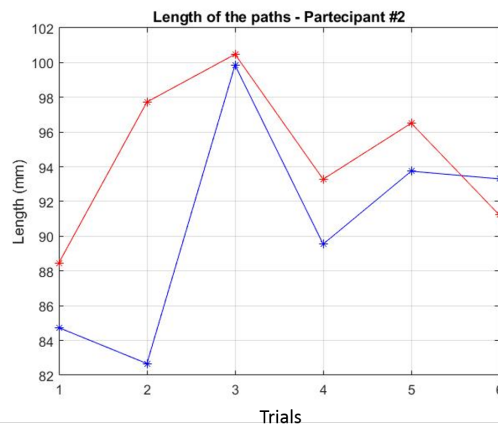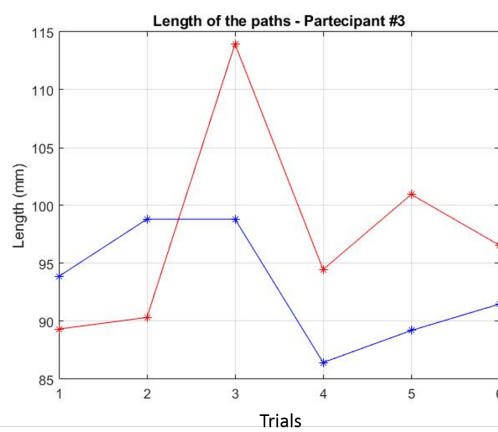
Figure 5.2: Lenghts (in mm, vertical axis) of each path in all trials (horizontal axis) of each participant.

5.2 Discussion

In this section, a few considerations regarding the results presented will be displayed.

In all the trials, the orifice (or its proximity) was reached. This means **the prototype can steer and enter a soft tissue structure** and reach points **turning and curving**. The prototype has then proved to be **axially and torsional stiff**, but **bendable** at the same time.

The participants were able to reach the proximity of the orifice when only helped by the visual support. This can be labeled as a great result, considering the users were 'blind' and only followed the path displayed. The **path proves to help proceeding towards the goal**, even if it's still not perfect. This is also because of a limitation of the bladder model, whose orifice doesn't match the one used as the target in the design of the path planning strategy. This is a situation that always happen in real cases, due to the deformability of soft tissue. Moreover, the final position of the targets appears to be moved in the different trials, which was expected considering the phantom is a soft tissue model and so can be easily shifted when inserting the prototype, which leads to a partial distortion of the phantom.

Regarding the participants pushing to insert the prototype and not following the curves of the urethra: this is due to the lack of vision of the position inside the urethra and the lack of haptic feedback. Integrating an endoscopic camera in the prototype could help solve the problem. In fact, seeing the urethra tortuous anatomy could lead to better decisions of the prototype.

The lower lengths of the paths recorded in the visual guidance group are explained as in this mode the participants were deciding their move-

ment without having to be told where to go. Therefore, they were sticking to the path on the screen without any chance of mistake (i.e. going right when asked to go towards left). A Student's t-test has been performed to see the relevance of this difference in the paths. The *p-value* regarding each participant's trials can be seen in Table 5.6. The test result is that the difference between the lengths is non-significative for all the participants.

Table 5.6: P-values.

p-value		
#1	#2	#3
0.388	0.847	0.86

Some limitations were noticed in the setup and were responsible for imperfect data collection. First, the Aurora sensor failed after few trials when outside the prototype. Therefore, we had to put it reversed inside of the tip. The recordings are then relative to a point $\sim$1 cm ahead/before the tip end. Those experiments have been done as a proof of concept to test the prototype segments' movements and path inside the bladder. They are not clinical-safe and thus the accuracy isn't. Moreover, the stepper motors don't guarantee a perfectly smooth movement. Another problem that emerged during the trials is that the driving cables running inside the grooves of the prototype broke several times

5.3 Possible future improvements and developments

In order to manage the problems stated before, some considerations can be done to **improve the setup**.

Regarding the breakage of the cables, as they have a strength of 1770 MPa (=1770 N/mm^2) is not possible that the cause of the breakage is

the force of pulling. The most probable cause is then the friction caused by the pulley material in contact with the cables. A smoother material could be investigated.

As the problem of finding the UO is very common during fURS, one of the possible future developments could be the introduction of a Neural Network (NN) able to detect automatically the UO during the scanning. This could be a support to the path performed by the robotized prototype. In fact, the prototype will be soon integrated with an endoscopic camera. The prototype could follow the pre-operatively designed path for only a percentage of it. At this point, the scope would start scanning in circular directions to detect the UO. In case it is detected, the device will change the path accordingly. In case it's not, it will continue for a few steps along the pre-determined path and then scan again. The possible drawback of this solution could be the availability of data. In fact, to train a robust NN and reach a good accuracy a large number of images would be necessary. This is also one of the reasons why this hasn't been done during this thesis. A CNN (Convolutional Neural Network) to detect UO has already been made by X. Peng et. al. [1]. They used resectoscopy images for the training and ureteroscopy ones for the testing of the NN. Data augmentation strategies were used to capture more features. Evaluation scores (such as precision, accuracy, etc.) show that using a real-time NN for automatic detection of UO can bring promising results. Integrating one in our flexible prototype strategy could then lead to a real-time automatic correction of the path.

Another possible problem is that, if the urethra is not designed almost perfectly in the model used to create the path, this one will make the device hit the lumen walls. Plus, as the diameter of the urethra is almost as big as the one of the ureteroscope, it is inevitable to have contact between the device and the lumen. Therefore, a way to solve this problem

could be the integration of force sensors. When the user overcomes the threshold set as the value bearable by the walls without being injured, the sensor would cause an alert signal. This could help in correcting the path according to the anatomy of the urethra and prevent the lumen from being damaged. Micro pressure sensors are already designed for catheter-like solution. In our case, more sensors should be positioned along the external part of the segments. One example already available on the market is the IntraSense ® [83] series of pressure sensors. Their size is 750μm $\times$ 220μm $\times$ 75μm, which allow to locate them easily on the walls without the creation of any significant protrusion.

6

Conclusions

An innovative prototype of ureteroscope and a path planning strategy for it have been studied in this research. As many surgeons struggle in finding the ureter orifice during ureteroscopy, the visual support of a pre-operative customized path aims in easing the difficulties of this task, in reducing the doctor's burden and, possibly, in the avoidance a cystoscopy.

Experiments have been conducted to understand if human control could easily guide the prototype tip, if the robot mechanical limits were properly included in the path, if following the strategy and receiving feedback from the visual support were important for improvements in time and accuracy. Conclusions regarding those aspects will be here reported.

The prototype was steered successfully inside the bladder model and towards the target. It has then proved to possess axial and torsional stiffness and to be flexible at the same time. It can bend up to 120°, which is more than enough for the task required in this research.

The participants, after some practice, felt intuitive to control the

steering of the prototype tip and gained awareness along the trials. The visual support of the path present on the screen made the participants guide the scope tip successfully inside the bladder and in the proximity of the target set. Moreover, having a pre-designed path to follow made people control more precisely the tip, resulting in a lower distance travelled by the tip.

The experiments pointed-out also some limitations of the setup and some ideas for future development. Another material for the motors pulley should be investigated, as the one used now causes friction and cause breakage of the prototype driving cables. Force sensors can be integrated in the tip of the scope, to alert in case an unbearable force is sensed when the robot is in contact with patient's anatomy. Endoscopic cameras will surely be integrated in a future version of the prototype. This could be even more useful if also a neural network for automatic orifice detection is designed.

To conclude, **progress has been made in the research of a ureteroscope prototype and of its path planning**, which, at the knowledge of this author, was never done before. Despite the improvements needed to implement the path planning strategy and to use the prototype in a clinical case situation, some promising results have emerged in this research. Modeling the morphological parameter of bladder from the CT scans of a patient has led to the creation of **customizable path planning** strategies. A pre-operative path has proved to guide all three participants enter the bladder and reach the proximity of the target. In a real-case scenario this could make the surgeon avoid the cystoscopy. The **prototype** designed has proved to be **reliably controllable, to steer in 3 dimensions and to be bendable up to 120°**.

The experiments and the study conducted by this researcher leave now the door open for future improvements. It would be interesting to

test the prototype withstand of loads, to integrate a force sensor and an endoscopic camera. Camera's information could then be integrated in the path planning strategy for its real-time modification.

Bibliography

[1] Michelle jo Semins and Brian R. Matlaga. "Medical evaluation and management of urolithiasis". In: *Therapeutic Advances in Urology* 2.1 (2010), pp. 3–9. ISSN: 17562872. DOI: 10.1177/1756287210369121.

[2] Francesco Porpiglia. *Manuale di Urologia*. Ed. by Minerva Medica. 2015th ed. Torino, 2015.

[3] Benjamin W. Turney et al. "Trends in urological stone disease". In: *BJU International* 109.7 (2012), pp. 1082–1087. ISSN: 14644096. DOI: 10.1111/j.1464-410X.2011.10495.x.

[4] José Manuel Reis Santos. "Ureteroscopy from the recent past to the near future". In: *Urolithiasis* 46.1 (2018), pp. 31–37. ISSN: 21947236. DOI: 10.1007/s00240-017-1016-8. URL: http://dx.doi.org/10.1007/s00240-017-1016-8.

[5] Victoriano Romero, Haluk Akpinar, and Dean G Assimos. "Kidney Stones: A Global Picture of Prevalence, Incidence, and Associated Risk Factors". In: *Rev Urol* 12.2 (2010), pp. 86–96. DOI: 10.3909/riu0459. URL: https://www-ncbi-nlm-nih-gov.proxy.library.upenn.edu/pmc/articles/PMC2931286/pdf/RIU012002%7B%5C_%7D0e86.pdf.

[6] Saeed R. Khan et al. "Kidney stones". In: *Nature Reviews Disease Primers* 2 (2016). ISSN: 2056676X. DOI: 10.1038/nrdp.2016.8.

[7] *slideshow-kidney-stones-overview @ www.webmd.com*. URL: https://www.webmd.com/kidney-stones/ss/slideshow-kidney-stones-overview.

[8] Riaz Agha and Gordon Muir. "Does laparoscopic surgery spell the end of the open surgeon?" In: *Journal of the Royal Society of Medicine* 96.11 (2003), pp. 544–546. ISSN: 01410768. DOI: 10.1258/jrsm.96.11.544.

[9] Dzelaludin Junuzovic et al. "Evaluation of extracorporeal shock wave lithotripsy (ESWL): Efficacy in treatment of urinary system stones". In: *Acta Informatica Medica* 22.5 (2014), pp. 309–314. ISSN: 19865988. DOI: 10.5455/aim.2014.22.309-314.

[10] Prahara Yuri et al. "Meta-analysis of Optimal Management of Lower Pole Stone of 10 - 20 mm: Flexible Ureteroscopy (FURS) versus Extracorporeal Shock Wave Lithotripsy (ESWL) versus Percutaneus Nephrolithotomy (PCNL)". In: *Acta medica Indonesiana* 50.1 (2018), pp. 18–25. ISSN: 01259326.

[11] Patrick Jones et al. "Percutaneous Nephrolithotomy in Patients With Chronic Kidney Disease: Efficacy and Safety". In: *Urology* 108 (2017), pp. 1–6. ISSN: 15279995. DOI: 10.1016/j.urology.2017.05.019. URL: https://doi.org/10.1016/j.urology.2017.05.019.

[12] Robert M. Geraghty et al. "Ureteroscopy is more cost effective than shock wave lithotripsy for stone treatment: Systematic review and meta-analysis". In: *World Journal of Urology* 36.11 (2018), pp. 1783–1793. ISSN: 14338726. DOI: 10.1007/s00345-018-2320-9. URL: https://doi.org/10.1007/s00345-018-2320-9.

[13] D. Georgescu et al. "Ureteroscopy - First-line treatment alternative in ureteral calculi during pregnancy?" In: *Chirurgia (Romania)* 109.2 (2014), pp. 229–232. ISSN: 1842368X.

[14] Nicholas J. Rukin et al. "Tips and tricks of ureteroscopy: Consensus statement part I. Basic ureteroscopy". In: *Central European Journal of Urology* 68.4 (2015), pp. 439–446. ISSN: 20804873. DOI: 10.5173/ceju.2015.605a.

[15] Natalie Zelenko et al. "Normal Ureter Size on Unenhanced Helical CT". In: *American Journal of Roentgenology* 182.4 (2004), pp. 1039–1041. ISSN: 0361803X. DOI: 10.2214/ajr.182.4.1821039.

[16] Adnan Gücük et al. "Does ureteral access sheat usage lead to permanent damage in the ureter? A placebo controlled trial in a rabbit model". In: *Acta Cirurgica Brasileira* 33.5 (2018), pp. 408–414. ISSN: 16782674. DOI: 10.1590/s0102-865020180050000002.

[17] JOHN KOURAMBAS, ROBERT R. BYRNE, and GLENN M. PREMINGER. "Dose a Ureteral Access Sheath Facilitate Ureteroscopy?" In: *The Journal of Urology* 165.March (2001), pp. 789–793. ISSN: 0022-5347. DOI: 10.1097/00005392-200103000-00012.

[18] Francesco Porpiglia et al. "Ureteroscopy: is it the best?" In: *Urologia* 81.2 (2014), pp. 99–107. ISSN: 03915603. DOI: 10.5301/uro.5000076.

[19] Jessica Packer Puru Naidu and John G. Calleary Maheshi Samaraweera. "Modern Upper Urinary Tract Endoscopy". In: *Intech* i.tourism (2012), p. 13. ISSN: 18734359. DOI: 10.1016/j.colsurfa.2011.12.014. URL: http://dx.doi.org/10.1039/C7RA00172J%7B%5C%%7D0Ahttps://www.intechopen.com/books/advanced-biometric-technologies/liveness-detection-in-biometrics%7B%5C%%7D0Ahttp://dx.doi.org/10.1016/j.colsurfa.2011.12.014.

[20] Petrisor Geavlete, Razvan Multescu, and Bogdan Geavlete. "Pushing the boundaries of ureteroscopy: Current status and future perspectives". In: *Nature Reviews Urology* 11.7 (2014), pp. 373–382. ISSN: 17594820. DOI: 10.1038/nrurol.2014.118.

[21] Farjaad M Siddiq. "Complications of Ureteroscopic". In: (), pp. 299–300.

[22] Farjaad M. Siddiq and Raymond J. Leveillee. "Complications of Ureteroscopic Approaches, Including Incisions". In: *Advanced Endourology* (2007), pp. 299–320. DOI: 10.1007/978-1-59259-954-7_18.

[23] Remzi Saglam et al. "A new robot for flexible ureteroscopy: Development and early clinical results (IDEAL Stage 1-2b)". In: *European Urology* 66.6 (2014), pp. 1092–1100. ISSN: 18737560. DOI: 10.1016/j.eururo.2014.06.047.

[24] *gastro @ www.olympus-global.com*. URL: https://www.olympus-global.com/technology/museum/endo/gastro.html?page=technology%7B%5C_%7Dmuseum.

[25] Maurizio Buscarini and Michael Conlin. "Update on flexible ureteroscopy". In: *Urologia Internationalis* 80.1 (2008), pp. 1–7. ISSN: 00421138. DOI: 10.1159/000111721.

[26] Steeve Doizi and Olivier Traxer. "Flexible ureteroscopy: technique, tips and tricks". In: *Urolithiasis* 46.1 (2018), pp. 47–58. ISSN: 21947236. DOI: 10.1007/s00240-017-1030-x. URL: http://dx.doi.org/10.1007/s00240-017-1030-x.

[27] Jaap D. Legemate et al. "Durability of Flexible Ureteroscopes: A Prospective Evaluation of Longevity, the Factors that Affect it, and Damage Mechanisms". In: *European Urology Focus* 5.6 (2019), pp. 1105–1111. ISSN: 24054569. DOI: 10.1016/j.euf.2018.03.001.

[28] Lily A. Whitehurst and Bhaskar K. Somani. "Semi-rigid ureteroscopy: indications, tips, and tricks". In: *Urolithiasis* 46.1 (2018), pp. 39–45. ISSN: 21947236. DOI: 10.1007/s00240-017-1025-7. URL: http://dx.doi.org/10.1007/s00240-017-1025-7.

[29] Maintenance Manual and Semi-rigid Ureteroscope. "Ureteroscope". In: (2000).

[30] "URF-P6 / P6R". In: (), pp. 6–8.

[31] "Flexible and Semi- Rigid Ureteroscopes Comprehensive Endourological Solutions". In: ().

[32] ACMI. "AUR ™ Flexible Ureteroscopes , DUR ® Durable Flexible Ureteroscopes / Choledochoscopes , and -735 Flexible Pediatric Cystoureteroscope Urétéroscopes souples". In: (2003).

[33] Olympus. "Olympus stone management". In: ().

[34] R. Wolf. "Instruction Manual: Flexible Fiber Ureterorenoscopes 7325.071 / 7325.076, Flexible 2-Channel Continuous Irrigation Laser URS 7326071 / 7326076". In: 0236 (2013), pp. 3–10.

[35] Storz. " Flexible Uretero-Renoscope Flex-X2s". In: (2020).

[36] Marc L.J.E. Paffen et al. "A comparison of the physical properties of four new generation flexible ureteroscopes: (de)flection, flow properties, torsion stiffness, and optical characteristics". In: *Journal of Endourology* 22.10 (2008), pp. 2227–2234. ISSN: 08927790. DOI: 10.1089/end.2008.0371.

[37] Man Cheong Lei and Ruxu Du. "A study on the bending mechanism of the flexible ureteroscope". In: *ICCAS 2010 - International Conference on Control, Automation and Systems* November 2010 (2010), pp. 2019–2023. DOI: 10.13140/2.1.4511.0727.

[38] Mert Ali Karadag et al. "Erratum to Flexible ureterorenoscopy versus semirigid ureteroscopy for the treatment of proximal ureteral stones: A retrospective comparative analysis of 124 patients [Urology Journal, Vol 12, No 4 (2015)]". In: *Urology Journal* 12.4 (2015), p. 2294. ISSN: 1735546X. DOI: 10.22037/uj.v12i4.3176.

[39] Ehab Mohamad Galal et al. "Retrospective comparative study of rigid and flexible ureteroscopy for treatment of proximal ureteral stones". In: *International Braz J Urol* 42.5 (2016), pp. 967–972. ISSN: 16776119. DOI: 10.1590/S1677-5538.IBJU.2015.0644.

[40] Erdal Alkan et al. "Flexible ureteroscopy can be more efficacious in the treatment of proximal ureteral stones in select patients". In: *Advances in Urology* 2015 (2015). ISSN: 16876377. DOI: 10.1155/2015/416031.

[41] H. Tanaka K. Suzumori, S. Iikura. *Flexible Microactuators for Miniature Robots.pdf*.

[42] Robert J. Webster, Allison M. Okamura, and Noah J. Cowan. "Toward active cannulas: Miniature snake-like surgical robots". In: *IEEE International Conference on Intelligent Robots and Systems* (2006), pp. 2857–2863. DOI: 10.1109/IROS.2006.282073.

[43] Christoff M. Heunis et al. "The ARMM System - Autonomous Steering of Magnetically-Actuated Catheters: Towards Endovascular Applications". In: *IEEE Robotics and Automation Letters* 5.2 (2020), pp. 704–711. ISSN: 23773766. DOI: 10.1109/LRA.2020.2965077.

[44] Sungwoong Jeon et al. "A Magnetically Controlled Soft Microrobot Steering a Guidewire in a Three-Dimensional Phantom Vascular Network". In: *Soft Robotics* 6.1 (2019), pp. 54–68. ISSN: 21695180. DOI: 10.1089/soro.2018.0019.

[45] Julien Catherine, Christine Rotinat-Libersa, and Alain Micaelli. "Comparative review of endoscopic devices articulations technologies developed for minimally invasive medical procedures". In: *Applied Bionics and Biomechanics* 8.2 (2011), pp. 151–171. ISSN: 17542103. DOI: 10.3233/ABB-2011-0018.

[46] L. Podsedkowski. "RobIn Heart 0, 1, and 3 - Mechanical construction development". In: *Bulletin of the Polish Academy of Sciences, Technical Sciences* 53.1 (2005), pp. 79–85. ISSN: 02397285.

[47] Giada Gerboni et al. "HelixFlex : bioinspired maneuverable instrument for skull base surgery". In: *Bioinspiration and Biomimetics* 10.6 (2015). ISSN: 17483190. DOI: 10.1088/1748-3190/10/6/066013.

[48] Awaz Ali et al. "Catheter steering in interventional cardiology : Mechanical analysis and novel solution". In: 233.12 (2019), pp. 1207–1218. DOI: 10.1177/0954411919877709.

[49] Kniji Asano et al. "Multijoint Inspection Robot". In: *IEEE Transactions on Industrial Electronics* IE-30.3 (1983), pp. 277–281. ISSN: 15579948. DOI: 10.1109/TIE.1983.356738.

[50] Paul W.J. Henselmans et al. "The MemoSlide: An explorative study into a novel mechanical follow-the-leader mechanism". In: *Proceedings of the Institution of Mechanical Engineers, Part H: Journal of Engineering in Medicine* 231.12 (2017), pp. 1213–1223. ISSN: 20413033. DOI: 10.1177/0954411917740388.

[51] Svenja Tappe et al. "Towards a follow-the-leader control for a binary actuated hyper-redundant manipulator". In: *IEEE International Conference on Intelligent Robots and Systems* 2015-Decem (2015), pp. 3195–3201. ISSN: 21530866. DOI: 10.1109/IROS.2015.7353820.

[52] Alessandro Gasparetto, Paolo Boscariol, Albano Lanzutti, Renato Vidoni. *Path Planning and Trajectory Planning Algorithms: A General Overview*. September 2017. 2015, pp. 3–27. ISBN: 9783319147055. DOI: 10.1007/978-3-319-14705-5.

[53] Liang Yang et al. "Survey of Robot 3D Path Planning Algorithms". In: *Journal of Control Science and Engineering* 2016 (2016). ISSN: 16875257. DOI: 10.1155/2016/7426913.

[54] E. W. Dijkstra. "A Note on Two Problems in Connexion with Graphs". In: *Vision Research* 6.2 (1966), pp. 269–271. ISSN: 00426989. DOI: 10.1016/0042-6989(66)90039-3.

[55] Harika Reddy. "PATH FINDING - Dijkstra's and A* Algorithm's". In: *International Journal in IT and Engineering* (2013), pp. 1–15.

[56] Steven M. LaValle. "Rapidly Exploring Random Tree". In: (316), p. 400.

[57] Disha Shah. "Path Planning for Mobile Robots using Iterative Artificial Potential Field Method". In: *International Journal of Computer Science Issues* 8.4 (2011), pp. 28–32. ISSN: 1694-0784.

[58] Harsimrat Singh et al. "Robotic Surgery Improves Technical Performance and Enhances Prefrontal Activation During High Temporal Demand". In: *Annals of Biomedical Engineering* 46.10 (2018), pp. 1621–1636. ISSN: 15739686. DOI: 10.1007/s10439-018-2049-z.

[59] Yucheng He et al. "Endoscopic path planning in robot-assisted endoscopic nasal surgery". In: *IEEE Access* 8 (2020), pp. 17039–17048. ISSN: 21693536. DOI: 10.1109/ACCESS.2020.2967474.

[60] Fang Liu et al. "3D trajectory planning algorithm for organ groups and irregular obstacles with application for prostate brachytherapy". In: *IEEE International Conference on Automation Science and Engineering* 2017-Augus (2017), pp. 1420–1424. ISSN: 21618089. DOI: 10.1109/COASE.2017.8256302.

[61] Zeyu Zeng et al. "Approach and control for robot assisted sinus surgery". In: *2017 IEEE International Conference on Robotics and Biomimetics, ROBIO 2017* 2018-Janua (2018), pp. 1–6. DOI: `10.1109/ROBIO.2017.8324545`.

[62] Yan-jiang Zhao et al. "3D Motion Planning for Robot-Assisted Active Flexible Needle Based on Rapidly-Exploring Random Trees". In: 3.5 (2015), pp. 360–367. DOI: `10.12720/joace.3.5.360-367`.

[63] Tariq Bahwini, Yongmin Zhong, and Chengfan Gu. "Path planning in the presence of soft tissue deformation". In: *International Journal on Interactive Design and Manufacturing (IJIDeM)* 13.4 (2019), pp. 1603–1616. ISSN: 1955-2505. DOI: `10.1007/s12008-019-00574-7`. URL: `https://doi.org/10.1007/s12008-019-00574-7`.

[64] Yan-jiang Zhao et al. "3D Dynamic Motion Planning for Robot-assisted Cannula Flexible Needle Insertion into Soft Tissue Regular Paper". In: (2016), pp. 1–11. DOI: `10.5772/64199`.

[65] Costanza Culmone et al. "Exploring non-assembly 3D printing for novel compliant surgical devices". In: *PLoS ONE* 15.5 (2020), pp. 1–21. ISSN: 19326203. DOI: `10.1371/journal.pone.0232952`. URL: `http://dx.doi.org/10.1371/journal.pone.0232952`.

[66] TU Delft. *BITE-Bio-Inspired Technology*. URL: `https://www.bitegroup.nl/`.

[67] TU Delft. *Delft University of Technology*. URL: `https://www.tudelft.nl/`.

[68] *Stepper Motor Datasheet*. URL: `https://datasheetspdf.com/pdf-file/1260602/Schneider/NEMA17/1`.

[69] Costanza Culmone, Gerwin Smit, and Paul Breedveld. "Additive manufacturing of medical instruments: A state-of-the-art review". In: *Additive Manufacturing* 27.October 2018 (2019), pp. 461–473. ISSN: 22148604. DOI: `10.1016/j.addma.2019.03.015`. URL: `https://doi.org/10.1016/j.addma.2019.03.015`.

[70] Digital Micromirror Device et al. "Digital Light Processing Overview of additive manufacturing process". In: (2018).

[71] "Let us print your part! 1". In: (), p. 500.

[72] Robert McNeel. *Rhino 6*. 2020. URL: `https://www.rhino3d.com/` (visited on 08/17/2020).

[73] *www.medicinapertutti.it/argomento/vescica-urinaria/*. URL: `https://www.medicinapertutti.it/argomento/vescica-urinaria/`.

[74] BWH. *Index @ Www.Slicer.Org*. URL: `http://www.slicer.org/`.

[75] *Find_the_intersection_of_a_line_with_a_plane @ rosettacode.org*. URL: https://rosettacode.org/wiki/Find%7B%5C_%7Dthe%7B%5C_%7Dintersection%7B%5C_%7Dof%7B%5C_%7Da%7B%5C_%7Dline%7B%5C_%7Dwith%7B%5C_%7Da%7B%5C_%7Dplane.

[76] *Ultimaker-3 @ Ultimaker.Com*. URL: https://ultimaker.com/en/products/ultimaker-3.

[77] Aurora NDI. "Aurora V3 User Guide". In: February 2014 (2014).

[78] Aurora NDI. "Data Sheet 610090". In: October (2019), pp. 2–5.

[79] University College of London. *Scikiy-surgerynditracker*. URL: https://github.com/UCL/scikit-surgerynditracker.

[80] Aurora Needle. "Aurora Needle, 2-Part, 21G/150 mm, Chiba". In: 610062 ().

[81] Eric Poulin et al. "Fast, automatic, and accurate catheter reconstruction in HDR brachytherapy using an electromagnetic 3D tracking system". In: *Medical Physics* 42.3 (2015), pp. 1227–1232. ISSN: 00942405. DOI: 10.1118/1.4908011.

[82] Yu Qi et al. "Electromagnetic tracking performance analysis and optimization". In: *2014 36th Annual International Conference of the IEEE Engineering in Medicine and Biology Society, EMBC 2014* (2014), pp. 6534–6538. DOI: 10.1109/EMBC.2014.6945125.

[83] *intrasense @ www.si-micro.com*. URL: https://www.si-micro.com/products/in-vivo-sensors/intrasense.html.

[84] Alfred M. Franz et al. "Electromagnetic tracking in medicine -A review of technology, validation, and applications". In: *IEEE Transactions on Medical Imaging* 33.8 (2014), pp. 1702–1725. ISSN: 1558254X. DOI: 10.1109/TMI.2014.2321777.

[85] Jack B. Kuipers. "SPASYN—An Electromagnetic Relative Position and Orientation Tracking System". In: *IEEE Transactions on Instrumentation and Measurement* 29.4 (1980), pp. 462–466. ISSN: 15579662. DOI: 10.1109/TIM.1980.4314980.

[86] Frederick H. Raab et al. *Magnetic Position and Orientatation Tracking System*. 1979. DOI: 10.1109/TAES.1979.308860.

[87] Kurt Schicho et al. "Stability of miniature electromagnetic tracking systems". In: *Physics in Medicine and Biology* 50.9 (2005), pp. 2089–2098. ISSN: 00319155. DOI: 10.1088/0031-9155/50/9/011.

[88] Ziv Yaniv et al. "Electromagnetic tracking in the clinical environment". In: *Medical Physics* 36.3 (2009), pp. 876–892. ISSN: 00942405. DOI: 10.1118/1.3075829.

[89] NDI. "Aurora Micro 6DOF Sensor Tool, 0.8 x 9 mm". In: 610059 (), pp. 9–10.

[90] Polhemus. *Index @ Www.Slicer.Org.* 2020. URL: https://polhemus.com/applications/electromagnetics/.

Appendix - Electromagnetic Tracking

The tracking of the prototype tip for the validation of the path computed has been realized thanks to Electromagnetic (EM) tracking. In computer-assisted interventions a common need is to gain the knowledge of the 3D localization of the instrument, called tracking. When the surgery performed is open, optical tracking solves the problem. However, if there isn't a free line-of-sight, markers cannot be applied. Therefore, an electromagnetic (EM) tracking system is used [84]. It performs the tracking of small EM sensors in a known EM field. This technique emerged in the late '70s thanks to Kuipers [85] and Raab [86] but has drowned interest in clinical applications only in the last two decades [87]. The main concern in clinical applications is the distortion of the magnetic field produced by ferromagnetic materials, included in instrumentation such as CT or MRI scanners [88]. This makes measures less accurate. Nowadays, the most common models are the Medical Aurora® (Northern Digital Inc.) [89] and the Pholemus one [90].

EM tracking exploits the response of magnetic sensors to a magnetic field of known geometry. This way, the position and orientation of the sensors can be known. The essentials needed to perform this technique are a field generator (FG), magnetic sensors (and their interface unit),

and a system control unit that interfaces with a computer.

To obtain the measurements of position and orientation at least three different fields of known geometry are needed. There isn't a standard FG, but they are the most widespread. Nowadays also flat FGs are available, they are positioned under the patient and limit distortion shielding the magnetic field. Differently, mobile field generators can be placed close to the region of interest, gaining the advantage of having a strong field where needed. In fact, a stronger field corresponds to a better output signal.

The physical property measured by magnetic sensors is the magnetic flux Φ [Tesla (T)], which is the component of magnetic flux density $\overrightarrow{B}$ that passes through a surface. As the sensors measure the gradient of a magnetic field, inhomogeneous magnetic fields are needed [84]. There are two types of sensors used to measure the magnetic flux: search coils (which need AC -Altermatin Current- fields) and fluxgate sensors (which uses pulsed DC -Direct Current- fields). Acquiring three measurements, when three different magnetic fields are applied, a nonlinear system of equations can be derived and solved. This allows us to get the position of the sensor. When sensors contain only one inductor, they are 5 DOFs sensors. This is because a magnetic dipole (as the one inside the sensor's inductor) is axially symmetric. In 6 DOFs instruments, two inductors are combined in one sensor.

Depending on the specific application, the most suitable EM tracker should be selected. The parameters that need to be taken into account are [88]:

- Refresh rate [Hz]
- Concurrency of sensors for different tools
- Working volume [m^3]

- Obtrusiveness (wired vs wireless sensors)

- Completeness (5DoF vs 6DoF)

- Accuracy

- Robustness against the environment.